Connections between the electron-energy-loss spectra, the local electronic structure, and the physical properties of a material: A study of nickel aluminum alloys

David A. Muller
School of Applied and Engineering Physics, Cornell University, Ithaca, New York 14853
and Bell Laboratories, Lucent Technologies, Murray Hill, New Jersey 07974

David J. Singh
Naval Research Laboratories, Code 6691, Washington, DC 20375

John Silcox
School of Applied and Engineering Physics, Cornell University, Ithaca, New York 14853
(Received 13 May 1997; revised manuscript received 4 December 1997)

The local electronic structure of a material can be determined from the energy-loss spectrum of a swift electron beam scattered through it. When the electron beam is focused down to the width of an atomic column, the electronic density of states (DOS) at an interface, grain boundary, or impurity site can be decomposed by site, chemical species and angular momentum. Here we discuss the use of electron-energy-loss spectroscopy (EELS) fine structure to provide insight into the origin of grain boundary and interfacial properties reported earlier [D. A. Muller *et al.*, Phys. Rev. Lett. **75**, 4744 (1995)] for Ni_3Al. We examine the electronic structure trends in Ni-Al compounds, both experimentally with the EELS measurements and theoretically, using *ab initio* band-structure calculations. The conditions under which the band-structure calculations can quantitatively reproduce the EELS measurements (and in particular, the question of just which local DOS is being measured) are addressed. Cyrot-Lackmann's moments theorem provides a framework to explain the systematic changes in the local DOS on alloying. The shape changes in the near-edge fine structure of both the Ni and Al *L* edges are readily understood by the sensitivity of the fourth moment of the local DOS to the angular character of the Ni-Al bonding. The language of bond-order potentials proved useful in linking shape changes in the DOS to changes in cohesion. The consequences for formation energies and ordering trends in the transition-metal–aluminum alloys are also discussed. [S0163-1829(98)04213-1]

I. INTRODUCTION

The fine structure in core edges determined with electron-energy-loss spectroscopy (EELS) (or x-ray absorption spectroscopy) can be used for a study of the electronic structure. In particular, for metals, these spectra can be related[1–6] to the unoccupied local densities of states (LDOS's) at the sites of the excited atoms. Various physical properties can provide insights into the electronic structure for extended crystals, but only recently have spatially resolved (3 Å) EELS measurements determined the local electronic structure changes that occur at the atomic scale at internal interfaces.[7–9,1] EELS studies can measure an effective LDOS from grain boundaries with structures that so far are too complex to simulate just as easily as for the bulk material. This opens up an experimental avenue for a determination of electronic structural features at extended defects such as grain boundaries, interfaces, and dislocations. Interpretation of such spectra and the relationship of the observations at defects to important physical properties is now an important goal, and indeed the ultimate goal of the work presented here.

A systematic investigation of the bulk electronic structure of the Ni-Al compounds is made. The comparison of the measured EELS spectra with band-structure calculations is useful for identifying the limits of the single-particle interpretation of the EELS spectra. Previous work with x-ray-absorption spectroscopy (XAS), which yields similar information (although not with comparable spatial resolution) shows that the XAS spectra of Ni (Ref. 3) and NiAl (Ref. 10) closely resemble the calculated ground-state densities of states (DOS's) for those materials. We would expect (and indeed find) similar agreement for Ni_3Al. The challenge is to understand these changes sufficiently well that we can predict and interpret the spectra from more disordered systems, such as grain boundaries, as well as we do for the bulk material.

The LDOS's can be calculated either from real-space calculations of clusters or from the band structures of periodic solids. All are equivalent in the appropriate limits, but it is often easier to obtain the fine details of the energy spectrum from the band-structure methods.[11] Many of the trends seen in the present EELS measurements can be deduced from band-structure calculations already present in the literature, provided the LDOS's, partitioned by site and angular momentum, have been published. There is, however, a danger in comparing LDOS's calculated by different methods, or for different basis sets as there is no unique way of dividing up the charge in any system more complicated than an isolated atom—and as a consequence, no unique definition of a charge transfer. By calculating the oscillator strength, which is the experimentally measured quantity, instead of the LDOS, the sensitivity to the basis set chosen in the calculation is reduced.

The layout of this paper is as follows: A review of previ-

ous work is given in Sec. II. In Sec. IV, we lay out precisely which local density of states is measured in our EELS experiments, and how that may be connected to various electronic structure calculations. Section V deals with measurement and normalization of the EELS spectra. The corresponding spectra are simulated with *ab initio* calculations in Sec. VI A. We discuss the differences between the Kohn-Sham eigenvalues calculated with density-functional theory (DFT) and the measured quasiparticle excitations. The calculated oscillator strength is found to be in good agreement with experiment, suggesting that ''many-body'' corrections are small. This allows us to make quantitative measurements of the partitioned charges upon alloying. Rather than discuss the alloying trends in terms of charge transfers, we find that changes in the shape of the EELS spectra can be far more readily understood with the aid of Cyrot-Lackmann's moments theorem. This, and the connection between the shape of the LDOS and changes in cohesive energy, are given in Sec. VI A. We pay particular attention to the role of the fourth moment in controlling the magnitude of the hybridization pseudogap. Finally, in Sec. VIII, the consequences for other transition-metal alloys considered, and simple rules of thumb for segregation and alloy heats of formation, are suggested.

II. BACKGROUND

$L1_2$ and $B2$ nickel aluminides have been the subject of a variety of *ab initio* calculations.[12–22] Both cohesive and elastic properties have been reported. The trends in electronic structure from Ni to $NiAl_3$ were summarized in Hackenbracht and Kubler.[13] Calculated bulk and shear modulii can be found in Refs. 20 and 21. Tight-binding models also have been used to model the Ni-Al phase diagram.[23]

There have been several previous electronic structure calculations of Ni_3Al (Refs. 13,17–19, and 22) and NiAl (Refs. 12–16) in which densities of states can be found. The work of Hackenbrackt and Kubler[13] provides a good overview of the trends in cohesive energy from Ni to NiAl. While bulk Ni and Al have been well characterized,[24,3,25] there have been only a few studies of the unoccupied DOS of the Ni-Al alloys.[15,10,26] Of these, the most relevant to the present work is a comparison of the XAS fine structure of Ni and NiAl by Pease and Azaroff,[10] showing that the Ni L edge in NiAl is flatter and broader at the onset than than in pure Ni. Pease also showed that the splitting of L_3 into two peaks could be understood in terms of the single-particle density of states obtained from augmented-plane-wave calculations.[27] EELS measurements were made more recently by Botton and co-workers[28,29] and D. A. Muller and co-workers[30–32] which confirmed these trends.

C. H. Müller *et al.*[33] compared measured x-ray emission spectra with band-structure calculations of transition metal aluminides from VAl to NiAl in the $B2$ structure. By keeping the aluminum content and geometries fixed, they were able to observe the changes in band filling as the atomic number of the transition metal was increased. Similar work on $B2$ Fe, Co, and NiAl was also performed by Botton *et al.*[29] using EELS. Although these aluminides all have a similar band structure, differing mainly in the position of the Fermi level, a strong nonrigid-band behavior is observed even for small changes in stoichiometry and structure.[34] Historically, these alloys have been analyzed in terms of a rigid band picture (a view that Mott cautioned against, even as he used it for explaining the magnetic properties of the Ni-Al system[35]). Central to the rigid-band picture for the intermetallics is the concept of a charge transfer from Al to the transition metal, gradually filling up a well-defined d band, with increasing Al concentration. As simulations became more sophisticated, and experimental probes of the local DOS became available, it also became more difficult to reconcile these results with the rigid-band picture. For lack of a comparably simple model, much of the rigid-band language remained. Even early *ab initio* calculations of intermetallic compounds were analyzed in terms of charge transfers and band narrowing, with respect to the pure elements.[12] However, different experimental and theoretical techniques led to different conclusions: Moruzzi, Williams, and Janak[12] found a charge transfer from Al to Ni and a Ni d-band narrowing in NiAl. While Lui *et al.*[16] also concluded that the Ni d band is narrower in NiAl than pure Ni; they inferred a charge transfer of opposite sign, from Ni to Al. Using a moments-based analysis of electronic structure calculations, Carlsson[36] found the Ni d DOS to be broader in NiAl than pure Ni. Pease and Azaroff[10] and Botton and Humphreys[28] preferred to describe the charge transfer as being from Al to Ni. None of these analyses were wrong; they simply used different definitions. Most of the later works do mention that sp-d hybridization is significant, and it is in separating the effects of hybridization (i.e. bonding) and charge transfers that most of the complications arise.

Here we explore the consequences of changing both the concentration and structure of the alloys. In particular, we consider the systematic trends in the Ni-Al compounds from Al, NiAl, and Ni_3Al to Ni. In doing so we are able to make quantitative tests of concepts such as different definitions of charge transfers, the validity of the local charge neutrality (LCN) approximation, s-d hybridization, and the ability to infer changes in cohesive energy from changes in the EELS spectra. Here we report quantitative tests of the LCN approximation, and find, contrary to the claims of Botton *et al.*,[29] that it is indeed a good approximation for the Ni-Al system. (In fact, the LCN approximation allows a successful prediction of the core-level shifts in the Ni-Al system, a result which we show in a companion paper.[37])

The ordering trends in Ni-Al alloys have been discussed in terms of the strong sp-d hybridization between Ni and Al.[38,23]. The preference for Ni-Al pairs over Al-Al nearest neighbors can be readily explained by the effect of the sp-d hybridization on the fourth moment of the LDOS.[36] The fourth moment, in turn can be connected to changes in the cohesive energy through a bond-order formalism.[39–41] Analysis of the EELS spectra in terms of the moments theorem and bond-order expansions offers controlled approximations for working back from the measured electronic structure to the physical properties of a system. This approach not only avoids many of the ambiguities inherent in the descriptions based on charge transfers, but also allows a quantitative discussion of cohesive energy differences based on the observed changes in EELS spectra, an issue which is addressed in a companion paper.[42] In the following sections we discuss

the problems in defining a local charge (Sec. III), and determining which local charge is measured with EELS (Sec. IV).

III. LOCAL DENSITY OF STATES

The arbitrariness with which the charge in a solid can be divided up means there are many ways in which a (single-particle) local density of states or a charge transfer between atoms can be defined. The more familiar concept of a total (single-particle) density of states is, however, a unique quantity. The total density of states is given by

$$N(E)=\sum_{n,\vec{k}}\delta(E-E_{n,\vec{k}}), \tag{1}$$

which measures the number of eigenstates $E_{n,\vec{k}}$ between E and dE throughout the entire crystal [so the contribution of the eigenstate at $E=E_{n,\vec{k}}$ is $\delta(E-E_{n,\vec{k}})$ where n is the band index and $\vec{k}$ is the electron wave vector]. This is a useful for a perfect, periodic solid, but in any real material there might be defects, surfaces, or impurities which do not resemble the bulk. If the local potential at a defect were lower than in the bulk, an increased charge density might be expected in its vicinity. The total DOS gives no indication that such an effect might be occurring, or where in the material that change is.

We are, however, free to project the total density of states on to a local set of states and examine the overlap of each eigenstate $|n,\vec{k}\rangle$ with the local state $|i\rangle$. The probability of finding an electron in the eigenstate $|n,\vec{k}\rangle$ at site $|i\rangle$ is $|\langle i|n,\vec{k}\rangle|^2$, so the local contribution to the density of states from site $|i\rangle$ is

$$n_i(E)=\sum_{n,\vec{k}}|\langle i|n,\vec{k}\rangle|^2\delta(E-E_{n,\vec{k}}), \tag{2}$$

and the charge associated with the local state $|i\rangle$ is

$$\rho_i=2\int_{-\infty}^{E_F}n_i(E)dE, \tag{3}$$

where E_F is the energy of the highest occupied state and the factor of 2 is for spin degeneracy.[43–47]

Which local densities of states can be compared to EELS measurements?

The choice of the local basis $\{|i\rangle\}$ set is not unique. Consequently, there is no unique way of determining the charge associated with each local state. Since the local charges cannot be uniquely defined, neither can the charge transfers. Consequently, great care must be taken when comparing different theoretical and experimental results to ensure that the same definition is used throughout. In an EELS or XAS measurement, the observable quantity is the oscillator strength, which defines the local basis set. This is not a basis set that is suitable for any electronic structure calculation, although it can be connected to some of the more commonly used basis sets (see Sec. IV).

Much of the language of elementary chemistry[48,45] assumes that atomiclike orbitals can still be identified in systems more complicated than atoms (and it is only in a single-electron atom that they are eigenfunctions). The concepts of charge transfer, bonding, covalency, and ionicity are most easily defined in terms of an atomiclike basis, for which they were originally intended.[49] The separation of these effects (and their very meaning) are less clear with other choices of basis sets. While it is always possible to project a more complete basis set on to an atomiclike basis (as do Sanchez-Portal, Artacho, and Soler for a plane-wave basis[50]), the results are not always unique, as they depend on the shape and extent of the radial wave functions. (See Tables I and II of Segall *et al.*[51]).

It will be shown in Sec. IV that electron-energy-loss spectroscopy of core-level excitations provides a measurable quantity that is proportional to a LDOS defined by an atomiclike basis. Consequently, when charge and charge transfers are discussed in this paper, the atomic-orbital definitions are used.

However, the *ab initio* calculations of Sec. VI B use an augmented-plane-wave (APW) basis. In an APW calculation[34,52] space is divided into nonoverlapping spheres centered on each atom and the remaining interstitial region. A plane-wave basis set is chosen for the interstitial region and the basis functions inside the spheres are solutions of the radial Schrödinger equation (a radial wave function multiplied by spherical harmonics) which are matched at the sphere boundary to the plane waves of the interstitial region. Often, the LDOS associated with the atom is taken to be the total density of states projected onto its associated sphere (where it should be stressed that the choice of sphere radius is largely a matter of computational convenience, provided the spheres do not overlap).

The main problem with this definition is that the charge in the interstitial region is ignored. In elemental Al, if the sphere radius is chosen as $2.3a_0$ (The Bohr radius $a_0=0.529$ Å), then there are only 1.73 electrons per atomic sphere (see Sec. VI B). As Al has three valence electrons, the remaining 1.27 electrons/atom are in the interstitial region. The charge redistributions in the interstitial region can be just as important as changes inside the atomic spheres. For instance, Schultz and Davenport[53] have shown that if the Ni and Al charges in $B2$ NiAl are compared with the corresponding atomic charges in the pure elements (again using a radius of $2.3a_0$ for all spheres), then *both* the Ni and Al spheres in NiAl gain charge with respect to their elemental solids. The Al sphere also gains slightly more charge than does the Ni sphere. On the other hand, if the reference systems are chosen to be the free, neutral atoms of Ni and Al, then in NiAl, the Ni charge is increased and the Al charge is decreased.[20] Rather than this latter calculation being evidence of an Al to Ni charge transfer, the results of Schultz and Davenport,[53] and Fu and Yoo,[20] taken together, suggest only that there is more charge in the interstitial region in elemental Al than would be expected for the superposition of free, neutral Al atoms.

Even if the spheres were expanded to fill all space (such as in the atomic sphere approximation commonly used in the linear-muffin-tin method[54]), there is still an ambiguity in choosing the sphere size in an alloy. One possibility is to replace each Wigner-Seitz cell by a sphere of equal volume.[55] Another would be to assume the charge is uniformly distributed throughout the material and choose the

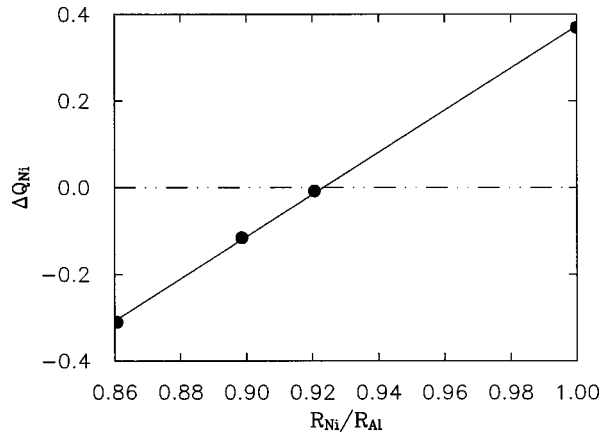

FIG. 1. The charge-transfer problem: Since there is no unique definition of a local density of states, there is also no unique definition for charge transfers between local states. To emphasize this point, and to caution against directly comparing EELS ''white lines'' against calculated charges (Ref. 94), we show the charge transfer from an atomic sphere surrounding a Ni atom in the $B2$ NiAl compound, calculated in the LMTO-ASA approximation (Ref. 54). The choice of the relative sphere sizes for the Ni and Al sites are a matter of computational convenience, rather than being a physically measurable property of the system. By altering the ratio of the Ni/Al sphere sizes we can change not only the magnitude, but also the sign of the Ni-Al charge transfer.

sphere radii so that the number of electrons in each sphere is equal to the ionic charge.[56] Nautiyal and Auluck[19] compared the two choices for Ni_3Al, and found that if equal sphere sizes are chosen then approximately 0.6 electron are transferred from the Al to Ni spheres. However, if the sphere radii are chosen using Anderson's prescription then the charge transfer is much smaller and in the opposite direction (0.02 electron are transferred from each of the Ni spheres to the Al sphere).

In short, in these atomic sphere approximations, the charge transfer can be defined to be almost anything, including no charge transfer at all. This ambiguity is illustrated in Fig. 1 where the charge transfer between Ni and Al is seen to change sign as the sphere sizes are changed.

In a single-particle picture, the increased electron density between the atoms is associated with the formations of covalent bonds (see, for instance, Refs. 45, 57, and 46). The electrons in the covalent bonds are understood to be shared between the two atoms, which means the number of electrons associated with each atom need not be altered when a bond is formed. It is very important to separate the concepts of charge transfers and bond formation (as very different simple models are used to describe each effect), especially in metals, where screening is very effective in reducing charge transfers, but bond formation can be quite pronounced.

A Linear combination of atomic orbitals as a basis set

To model (and separate) the effects of covalent bonding and charge transfers between atoms explicitly, the natural choice of basis set is a linear combination of atomiclike orbitals (LCAO). The basis functions are atomiclike, as they have same angular momentum dependence as the orbitals of a free atom, although the radial dependence may be quite different. The LCAO definition is a more chemically intuitive description of the charge per atom than dividing the electrons into fixed regions of space. First, it assigns the same number of electrons per atom to an elemental solid as it does to a free atom of the same species. Second, buildup of charge between atoms due to the formation of covalent bonds does not alter the number of electrons per atom in this definition. Only when there is an ionic character to the bonding does ρ [of Eq. (3)] change (This is not the case with ''muffin-tin'' charges). When charge transfers are discussed in later sections, the LCAO picture will be used, unless otherwise noted.

Can experimental measurements be made of the LCAO charges? As the definition involves possibly fictitious wave functions, the answer must be[1] ''not exactly.'' However, a very good approximation can be made. In an electron-energy-loss measurement of a core excitation (see Sec. IV), the unoccupied densities of state are projected on to a local basis defined by the initial core states. The resulting basis is localized close to the ion cores, where the *shapes* of the wave functions are determined more by the boundary conditions imposed by the ion core [$r\phi(r)\rightarrow 0$ as $r\rightarrow 0$] than by interactions with neighboring sites. Instead, only the normalization coefficient of the wave function can change when the environment of the atom is changed. It is this property which makes the experimentally measured EELS oscillator strength proportional to a LCAO density of states. The connection between the EELS oscillator strength and the LCAO LDOS will prove useful in analyzing the measured EELS spectra, and in developing simple models of the local electronic structure. Although it is traditional to assume that the oscillator strength is proportional to a LDOS and some prefactor that is purely atomic in nature, it should be expected (and it will be shown in Sec. IV) that this relationship cannot hold for every choice of the LDOS.

IV. THEORY OF CORE-LEVEL SPECTROSCOPY

In the first Born approximation, the partial cross section for the inelastic scattering of an electron wave packet (with initial group velocity v), undergoing a momentum transfer $\vec{q}$ and losing energy E,[58–60] is given by

$$\frac{d^2\sigma(E,q)}{dEdq}=\frac{8\pi e^4}{\hbar^2 v^2}\frac{1}{q}\sum_{i,f}|\hat{\epsilon}_q\cdot\langle f|\vec{r}|i\rangle|^2\delta(E-E_f+E_i)+\cdots \tag{4}$$

for small momentum transfers ($q\ll 1/r_c$, where r_c is a measure of the size of the core state) and $|i\rangle$ and $\langle f|$ are the initial and final states of the target. Here $\hat{\epsilon}_q$ is a unit vector in the direction of $\vec{q}$. The momentum transfer is a function of the detector geometry and in our work is restricted to small enough scattering angles that the dipole contribution dominates.

The comparable x-ray-absorption cross section is[59,61]

$$\sigma_{\rm abs}(E)=4\pi^2\alpha\omega\sum_f|\hat{\epsilon}\cdot\langle f|\vec{r}|i\rangle|^2\delta(\hbar\omega-E_f+E_i), \tag{5}$$

with $E=\hbar\omega$. The terms in the summation on the right-hand sides of Eqs. (4) and (5) are common to both EELS and

XAS, once it is realized that in EELS the direction of the momentum transfer $\hat{\epsilon}_q$ plays the same role as the polarization vector $\hat{\epsilon}$ does in XAS. These terms are then a function only of the specimen and not the probe used. As orientational effects in the bulk Ni-Al compounds are weak, the analysis can be simplified by assuming that the specimen is isotropic or polycrystalline, so all orientations to the beam are equally sampled—this removes the polarization dependence, replacing $\hat{\epsilon}\cdot\vec{r}$ with $\frac{1}{3}$. It is also convenient to factor out the specimen-dependent information in a dimensionless form known as the (optical) (Ref. 62) oscillator strength $F(E)$, which is defined as

$$F(E)=\frac{1}{3}\frac{2m}{\hbar^2}E\sum_{i,f}|\langle f|r|i\rangle|^2\delta(E-E_f+E_i). \tag{6}$$

Once the scattering geometry is determined, the same information can be obtained from EELS as from XAS. There is, however, a subtle difference in the energy dependencies of the EELS and XAS cross sections. If the EELS cross section is integrated over q, then the ratio of the x-ray cross section to EELS cross section (per eV, per atom) is[63]

$$\frac{\sigma_{\rm abs}(E)}{\sigma_{\rm EELS}(E)}=\frac{2\pi a_0}{\hbar c}E_0E\,\ln\left(\frac{4E_0}{E}\right). \tag{7}$$

The EELS cross section per Ni atom for an 860-eV energy loss of a 100-keV electron is roughly 10 b/eV which corresponds to mean free path $\lambda=1/\rho\sigma(E)$ of about 1 cm in Ni. Using Eq. (7), the mean free path for an 860-eV x ray in Ni is about 10 nm. While self-absorption effects are a serious problem for transmission XAS experiments in Ni alloys, they are not a problem for EELS measurements of core losses. This does not, however, mean that transmission EELS experiments can be performed on a 1-cm-thick piece of Ni, only that the multiple scattering corrections are different. Instead, the EELS cross section is strongly peaked at low energies, where the valence excitations provide the major contribution to the total inelastic cross section. The mean free path for the low-energy valence losses is roughly 80 nm, so it is multiple valence excitations that limit the usable thickness. (The elastic scattering is less of a problem at these depths, as it is still strongly peaked in the forward direction.) A swift electron traveling through a thin film is likely to experience both core losses and repeated valence losses, resulting in a convolution of the core edge with the low loss region. This multiple valence scattering does not have a large effect on the near-edge structure (see Fig. 4), and is readily corrected by deconvolution.[64] The different energy dependencies of the EELS and XAS cross sections make the two techniques very complementary. The rapid decrease in the EELS cross section with energy makes it very difficult to perform measurements at more than a few keV, an energy range where x-ray measurements become more practical.

A. Core-level transitions

The simplest model of the core-level oscillator strengths (for both EELS and XAS) is to consider only single-particle transitions.[65,66,5] In all but the shallowest of core-shell excitations, many-body effects can be treated as corrections to the single-particle transitions, so that the excitations can be labeled by their single-electron counterparts. In this work the excitations of interest are the $L_{2,3}$ edges in Al and Ni.[67] The initial states are $(|i\rangle=|2p_{1/2}\rangle,|2p_{3/2}\rangle)$. In a solid, the unoccupied states will not have a definite angular momentum, because the potential is no longer spherically symmetric. However the dipole selection rules ($\Delta l=\pm1$) restrict the final states to be of s-like ($l=0$) or d-like ($l=2$) symmetry.

For single-particle transitions the terms $F(E)$ can be recognized as being proportional to a LDOS, where the localized basis is determined by the shape of the core wave functions, and has the form $r|\phi_c\rangle=|r\phi_c\rangle$ where ϕ_c is the initial core state, $|i\rangle$:

$$F(E)\propto\sum_{all f}|\langle r\phi_c|f\rangle|^2\delta[E-(E_f-E_c)]. \tag{8}$$

Strictly speaking, Eq. (8) is a joint density of states. However, the core states are sufficiently localized with no band dispersion or structure, so the only nontrivial summation is over the final states. There are two unusual features if Eq. (8) is considered a LDOS. First, the basis chosen is not complete, as the core states are far more localized than the valence wave functions. As will be shown, this is less of a problem than might be expected. Second, the energies are measured with respect to the binding energy of the core state. This has the advantage for an experimentalist that the LDOS on a Ni site can be measured separately from the LDOS on a Al site as the core-level binding energies E_c are different for different elements.

Although the oscillator strength can be viewed as a LDOS in its own right, the basis set determined by the experiment is not one used in any electronic structure calculations. To make contact with theory, it is still necessary to relate the EELS oscillator strength to the basis sets used in simulations, such as either muffin-tin or atomiclike orbitals.

The approach taken in early work on x-ray-absorption spectroscopy[2] was to assume that the oscillator strength $F(E)$ could be factored into the desired partial density of states $d_{i,J}(E)$ and a (hopefully) slowly varying transmission function $T(E)$, which was a function of the probed atom, but not its local environment, i.e.,

$$F(E)=T(E)d_{i,J}(E). \tag{9}$$

This has been the traditional starting point for the interpretation of the near-edge XAS.[65,66] However, such a factorization is limited to a small number of special basis sets where the *shape* of the wave function is a function only of energy and angular momentum (see Appendix A). It cannot, for instance, be a function of crystal momentum $\vec{k}$; otherwise there will be cross-terms of the form $\langle f|\phi_{\vec{k}}\rangle\langle\phi_{\vec{k}'}|f\rangle$. More precisely, if the calculation is performed with a basis set $\{|\phi_{i,k,J}(E)\rangle\}$ that depends on energy (E), angular momentum J, a site in the unit cell (i), and some other parameter, say k, then the factorization of Eq. (9) is only possible if

$$|\phi_{i,k,J}(E)\rangle=c_k|\phi(E)_{i,J}\rangle. \tag{10}$$

A tight-binding basis of atomiclike orbitals trivially satisfies this condition. This is not the case for the basis sets of most modern linear methods, such as LMTO or LAPW. Neverthe-

less, if the core orbital is localized near the nucleus (as for deep core levels such as the Ni $2p$ state) then the important boundary conditions are the atomic ones, such as the radial wave function vanishing at the nucleus or orthogonality to the core levels. Then the shape of the wave function is determined only by the energy (and the electron density), so Eq. (10) is a very good approximation in practice, and is widely used (e.g., Lerch *et al.*[6]).

This factorization was obtained rigorously by Müller and Wilkins[4] for their APW method, since their basis satisfied Eq. (10) [Eqs. (3.5b) and (B4) in their paper]. It should be noted, however, that the atomiclike term $T(E)$ is a function of the sphere size chosen to project out the LDOS. [A smaller sphere size has a more slowly varying $T(E)$.] As the oscillator strength is a physically measurable quantity, it must be independent of the sphere size chosen in the calculation. This implies that there is a compensating normalization factor in the LDOS which cancels the sphere size dependence in $T(E)$ (by making the LDOS a function of the sphere size as well). A key point made by Müller and Wilkins is that the band structure or ''solid-state'' contribution is not given by the sphere-projected DOS, but rather by that DOS normalized by its single-atom DOS. This single-atom DOS is calculated with the same electron configuration as the solid, not a free atom, so it is not, in general, an experimentally measurable quantity.

B. Oscillator strength as a LDOS

In short, although a calculated LDOS may qualitatively resemble an XAS or EELS signal, for quantitative comparison with *ab initio* methods, the oscillator strength itself must be calculated. The oscillator strength can be considered as a LDOS [by using Eq. (8)]. It is also directly related to a LCAO basis, of the type used in tight-binding calculations [through Eq. (10)]. The transmission function $T(E)$ is then atomic in nature, and has the simple form

$$T=\frac{1}{3}\frac{2mE}{\hbar^2}|\langle\phi_{i,c}|\vec{r}|\phi_{i,J}\rangle|^2. \tag{11}$$

For Müller and Wilkin's APW method [or for any basis that satisfies Equation (10)], the transmission function has a more complicated energy dependence

$$T(E)=\frac{1}{3}\frac{2mE}{\hbar^2}|\langle\phi_{i,c}|\vec{r}|\phi_{i,J}(E+E_c)\rangle|^2. \tag{12}$$

For the linear methods, where the oscillator strength can be exactly related to the sphere-projected DOS, an approximate transmission function can be obtained from

$$T(E)\approx\frac{F_{i,J}(E)}{d_{i,J}(E)}. \tag{13}$$

For the LAPW calculations used in this work, the core wave functions are zero on the boundary of the muffin sphere, so only the radial portion of LAPW wave functions is needed as a basis for the LDOS and matrix elements.

Figures 2 and 3 show the ''atomic'' transmission functions obtained from Eq. (13) using the LAPW optical oscillator strengths and the LAPW LDOS for Ni and Al in different environments. The functions are smoothly varying in energy, and do not contain any vestiges of the rapidly changing band-structure features, showing Eq. (9) to be a good approximation for the Ni and Al L edges. However, the transmission function is different for different compounds and not independent of the local environment, as is often assumed. The differences in shape correlate more with the sphere radii chosen for the various calculations than changes in charge redistributions. For instance, in Fig. 2, $|r_{pd}(E)|^2$ for Ni_3Al is peaked at a higher energy than for Ni or NiAl, although the environment of Ni in Ni_3Al is expected to be intermediate between Ni and NiAl. The trend can be understood by noting that the sphere radius chosen for the Ni_3Al calculation was larger than those for Ni and NiAl, as was mentioned earlier.

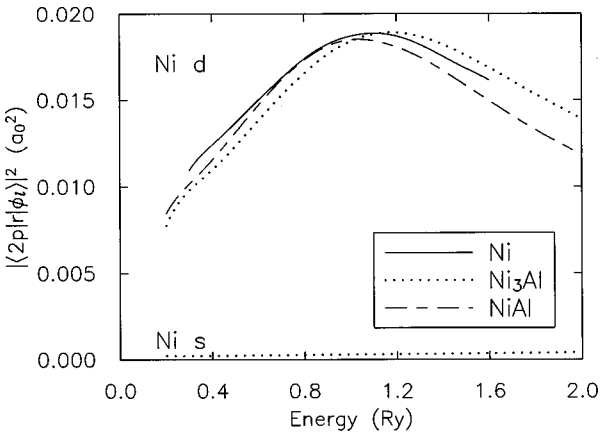

FIG. 2. The s and d transmission functions, $T_{2p,J=s,d}(E)$, for the Ni $L_{2,3}$ edge obtained from Eq. (13) using the LAPW optical oscillator strengths and the LAPW-projected LDOS for Ni and Al in different environments. Notice how much weaker the $2p\rightarrow s$ transition is than the $2p\rightarrow d$ transition.

Why are the $2p\rightarrow d$ transitions so much stronger than $2p\rightarrow s$ transitions in Ni? Here some insight can be gained from studying the wave functions of a free atom. The $2p$ and $3d$ wave functions are nodeless, while the $3s$ or $4s$ wave functions have nodes in the region of the $2p$ orbital leading to large cancellations in the radial integral $|\langle 2p||r||4s\rangle|$. For

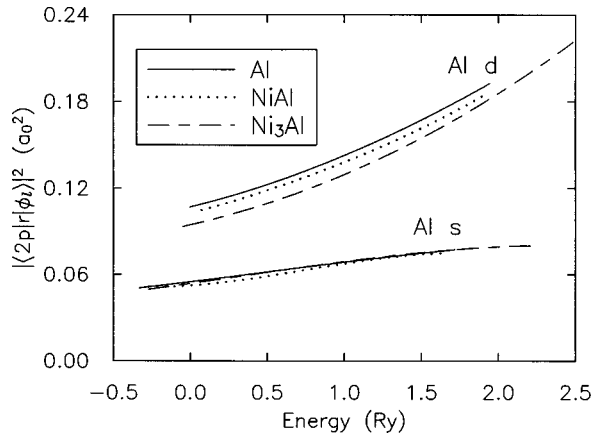

FIG. 3. The s and d transmission functions $T_{2p,J=s,d}(E)$ for the Al $L_{2,3}$ edge obtained from Eq. (13) using the LAPW optical oscillator strengths and the LAPW-projected LDOS for Al in different environments.

the L edge in a free Ni atom $|r_{p,d}/r_{p,s}|^2=129$. This effect is much less pronounced for an L edge in an Al atom, as neither the $3d$ nor $4s$ states are bound. Instead, both resemble continuum Coulomb wave functions ($|r_{p,d}/r_{p,s}|^2=0.5$).

V. EXPERIMENTAL METHOD

Details of the specimen preparation, instrumentation, and processing of the recorded spectra are given in Sec. V. Finally, the bulk spectra from the Ni-Al compounds are presented. The trends seen in these Ni and Al $L_{2,3}$ edges are the motivation for Sec. VI on bulk electronic structure.

A. Specimen preparation

Electron spectroscopy in a scanning transmission electron microscope (STEM) is performed in a transmission mode, usually with a small focused probe. The bulk specimens must be thinned to electron transparency (less than 100 nm and usually 20 nm). This is still much thicker than the absorption length for Ni and Al L-edge x rays (see Sec. IV). This means self-absorption corrections are important in transmission x-ray measurements but not in EELS.[68] The overall inelastic mean free path for a 100-keV electron is $\approx$80 nm, with almost all of the additional scattering due to valence and collective excitations. This plural scattering can be easily corrected by Fourier ratio deconvolution.[69] Elastic scattering does *not* change the shape of the energy-loss spectrum for the experimental conditions considered in this paper. It can only change the overall intensity. Consequently, the EELS signal from a ''thin'' film can be more representative of the bulk than the corresponding XAS measurement. An additional advantage of spectroscopy in an electron microscope is that the specimen can be imaged and regions with obvious defects can be examined separately. The high lateral spatial resolution (2–8 Å) means the specimen need only be defect free over distances as small as a few nanometers. Of course, very much larger areas are used to avoid finite-size effects.

Al thin films were deposited directly on to formvar grids by magnetron sputtering. This meant only one surface of the film was exposed to atmosphere when the specimens were transferred to the STEM. The nominal mass thickness was 20 nm, but grains as large as 50 nm were observed. The Al L edges were recorded on these larger grains where the surface oxide accounted for less than 5% of the probed volume. The Ni, NiAl, and Ni_3Al specimens were prepared for transmission electron microscopy by jet polishing with a 10% sulfuric acid solution in methanol.

B. Instrumentation

The Cornell VG-HB501A 100-kV STEM has a field emission gun with a 0.3-eV energy spread and is fitted with a McMullan style parallel electron-energy-loss spectrometer (PEELS).[70] This was installed as an upgrade to the standard VG Serial EELS. The bending magnet of the spectrometer has a dispersion of 1 eV/μm at the energy selection slits. By adding three quadrupole lenses after the slits, the energy dispersion can be increased by up to a factor of 100. The dispersed beam strikes an yttrium aluminum garnet scintillator which is optically coupled to a 512×512 pixel charge-coupled device (CCD). The resolution of the spectrometer is $\approx$0.1 eV (largely due to the spreading of the beam in the scintillator to $\approx$80 μm). As a large energy range was needed for recording the bulk spectra to allow accurate deconvolutions, the effective energy resolution was reduced to 0.8 eV. Since the spectrometer is not connected to the high-voltage supply of the microscope, it is sensitive to fluctuations in the beam voltage. Core-level shifts between different specimens could be determined to within 0.5 eV. Absolute energy measurements are accurate to about 1 eV as the low loss spectra must be recorded at a lower extraction voltage than the core loss spectra to prevent saturation of the CCD and damage to the scintillator. More accurate, absolute measurements of the core-level shifts will be given in a subsequent paper.[37]

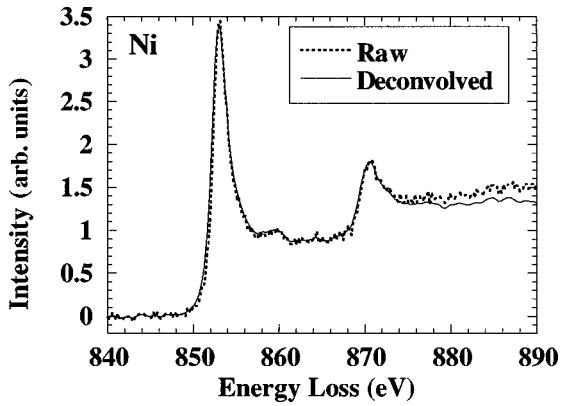

FIG. 4. Measured Ni $L_{2,3}$ EELS edge from a 15-nm-thick Ni film, before and after deconvolution. A power-law fit to the pre-edge intensity has been used to remove the background in the raw data. A Wiener filter with a signal to noise ratio of 50 was used to deconvolve the loss-low plural scattering. The spectrum was recorded with serial EELS.

C. Recording and processing of spectra

As the specimens were prepared by jet polishing, a thin surface oxide layer could sometimes be detected. Depending on the polishing conditions, and how long the specimen had been exposed to atmosphere, the oxide layers could be from 1 to 5 nm thick. This was a particularly severe problem for NiAl. Consequently many samples had to be rejected. Only specimens in which the 0-K edge could not be detected at the 5-at. % level were used. The possible presence of a surface oxide also limited the thickness of the sample studied to be more than 20 nm thick. This is one-fourth of the total inelastic mean free path in these materials, which makes the deconvolution of valence excitations from the core edges necessary.

The effect of this plural scattering is to convolve the core spectrum with the low-loss region of the energy-loss spectrum. As the scattering events are independent and follow a Poisson distribution, they can be deconvolved using the Fourier ratio method,[64,71] which was performed using a Wiener filter.[72] The Wiener deconvolution also corrects some of the differences in detector response and makes possible a comparison of spectra recorded from films of differing thicknesses.[73] As the interband and collective excitations peak at roughly 20-eV energy loss, plural scattering has little effect on the shape of L_3 near-edge structure, although it

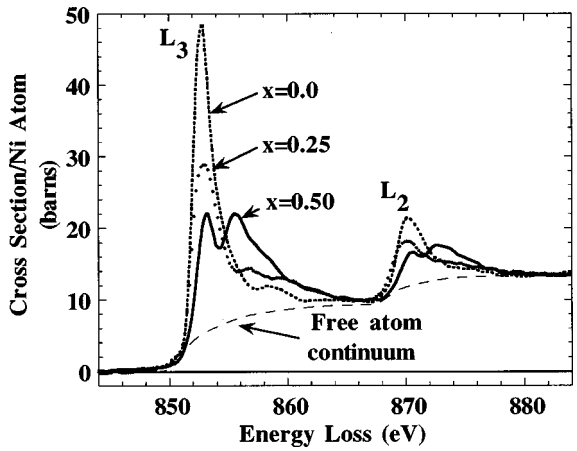

FIG. 5. Measured Ni $L_{2,3}$ edge (after deconvolution and background subtraction) for the $Ni_{1-x}Al_x$ system showing the decrease in height and broadening of the sharp peak (''white line'') at the onset of the L_2 and L_3 edges with increasing Al concentration. The spectra are scaled to the atomic Ni cross section (see text). The statistical errors in the measured spectra are indicated by the plotted line thickness. There is also a 2%–5% systematic error in the background subtraction.

does alter the background for the L_2 edge (see Fig. 4). The deconvolution is more important for data recorded with the parallel EELS than the serial EELS as the PEELS point-spread function (PSF) has a significant fraction of its intensity in the tails of the central peak. The SEELS PSF has a better apodization, but the lower count rates limit the resolution.

Another source of error is the background subtraction procedure. After the instrumental background and gain variations have been corrected, the remaining background is composed mostly of the tails of lower-energy edges and valence excitations which are traditionally modeled as a power law[59,69] (this can be rigorously shown for a hydrogenic system[59]). For energy losses larger than a few hundred eV, this is a reasonable approximation. However, care must be taken to fit the background well before the edge onset, particularly at large energy losses. The core-hole lifetime at large energy losses is very short, which has the apparent effect of convolving the spectrum with a Lorentzian. The tails of this Lorentzian can extend well before the edge onset and change the apparent slope of the background. The tails of the PEELS PSF has a similar effect. For this reason, we prefer to deconvolve the raw spectra before subtracting the pre-edge background (as this corrects the tails added by the PEELS PSF). The uncertainty in the background is single largest source of error in estimating the area and moments of a measured EELS curve. The larger the energy window of interest, the more serious the error.

D. Results of the EELS L-edge measurements in Ni-Al compounds

Processing of the Ni $L_{2,3}$ edges is considerably simpler than for the Al $L_{2,3}$ edges, as there are no nearby overlapping edges. The background subtracted and low-loss deconvolved Ni L edges are shown in Fig. 5. There are two peaks in each spectrum, as there are two nickel L edges, (L_2: $2p_{1/2} \rightarrow d_{3/2}$ and L_3: $2p_{3/2} \rightarrow d_{3/2}, d_{5/2}$) at 852- and 868-eV energy losses, respectively, which select excitations from the nickel $2p$ core orbitals to unoccupied states on the same nickel site.[74] As discussed in Sec. IV, the observed intensity is proportional to the LDOS with s-like ($l=0$) or d-like ($l=2$) symmetry in the conduction band. Transitions to $l=2$ states dominate by a factor of ~ 100 (Refs. 75, 76, and 4) (see also Figure 2).

TABLE I. Ni $L_{2,3}$ edge cross sections (in b per Ni atom) for the $Ni_{1-x}Al_x$ system. The range of integration is -5–35 eV from the Ni L_3 edge onset. The spectra are scaled to the Hartree-Slater cross section for atomic Ni calculated by Peter Rez.

x	I_x(b)	I_x/I_{Ni}
Ni	514 ± 10	1.000
Ni_3Al	506 ± 10	0.984 ± 0.04
NiAl	508 ± 10	0.988 ± 0.04
Ni_3Si	508 ± 10	0.988 ± 0.04[a]

[a]Ni_3Si spectrum from Ref. 114.

The uncertainties in film thickness and calibration of the efficiency of the detector make it very difficult to measure the cross sections on an absolute scale. These problems are shared with XAS, where knowledge of the film thickness and uniformity is even more limited due to the lack of spatial resolution. However, as pointed out by Müller and Wilkins,[4] well above the edge onset where the fine structure is damped out, the overall magnitude of a particular transition (e.g., the Ni L edge) is determined by its corresponding atomic transition (the extended fine structure oscillates about the atomic cross section). The implication is that the cross-section (per Ni atom) for a Ni L edge will always be asymptotic to the same value, irrespective of the environment of the Ni atom. This makes it possible to compare the relative changes in the shape of the Ni Ledges recorded in different materials.

If the edges are scaled so that they all match at energies well above the edge onset (see Appendix B), then all the spectra have the same intensity scale and thickness, and detector effects have been factored out. Thus comparisons of the relative cross sections per Ni atom can be made. The measurements can be placed on an absolute scale by noting that all the Ni spectra must match the atomic Ni cross section well beyond the edge onset. (The LAPW band structures discussed in Sec. VI B do not cover a wide enough energy range for a general comparison to be made.)

Figure 5 shows Ni L edges from various Ni-Al alloys after background subtraction and deconvolution of multiple scattering. The spectra are scaled to the Hartree-Slater (HS) cross section for a Ni atom[77] (supplied by P. Rez). The integrated cross sections, normalized by Eq. (B2), are given in Table I. The absolute values should not be taken too seriously as the atomic model is not appropriate close to the edge onset. However, it is very significant that although the shape of the spectra are very different for different alloys, the areas defined by Eq. (B2) are almost identical. As shown in Sec. IV, this area is proportional to the number of holes of $l=2$ character near the core of the Ni atom. Section IV further shows that $d\sigma_x(E)/dE$ is proportional to a tight-binding LDOS. This means that in a tight-binding description, the number of Ni d holes in the integration window does not

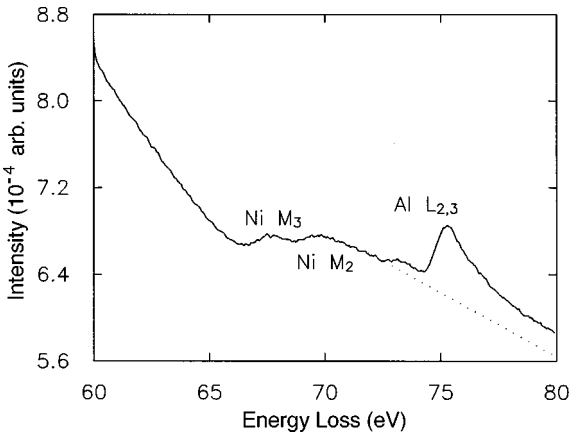

FIG. 6. Raw EELS spectrum of NiAl showing the overlap of the Ni $M_{2,3}$ edge with the Al $L_{2,3}$. The dotted line shows the extrapolated background for the Al L edge.

change by more than 2% upon alloying, and is the first hint that the alloying changes are not the result of intersite charge transfers (between atomic-like orbitals).

The Al $L_{2,3}$ at 72 eV overlaps with the Ni M edge at 67 eV (Fig. 6). The presence of a Fano resonance at the Ni M edge in Ni (Ref. 78) and Ni_3Al (but not NiAl) complicates the interpretation of the M edge, and makes the background subtraction more difficult. The Al L edge, however, is free of a Fano resonance, and there is little structure in the Ni M edge above 70 eV (i.e., near the Al L edge). A background-stripped Al L edge was obtained by first removing the pre-edge background from the Ni M, edge and then linearly extrapolating the tails of the Ni M edge, as is actual shape is unknown (although it contains no sharp features). The extrapolation is only a reasonable approximation near the edge onset. Consequently, a comparison of the measured and calculated Al L edge is restricted to within 6 eV of the edge onset.

Figure 7 shows the background-stripped Al $L_{2,3}$ edges for the $Ni_{1-x}Al_x$ system. The key feature of the spectra is the ''scooping out'' of the density of states near the edge onset which becomes more pronounced with increasing Ni concentration. This trend is not affected by errors in the background extrapolation, and will be discussed later in terms of s-d hybridization.

E. Summary

General techniques and precautions pertaining to the experimental measurement of EELS spectra have been given. The recording and processing of the Ni and Al EELS spectra that will be used in later sections were also described. The following trends were observed: The Al L edge develops a pronounced ''scooping out'' in intensity at the edge onset as the compounds become increasingly Ni rich. The Ni L edge became increasingly broader and flatter as the Al concentration is increased. However, the cross section per Ni atom for the near-edge region of the Ni L edge is the same, within experimental error, for Ni,Ni_3Al and NiAl. Given the relationship between the EELS oscillator strength and the LCAO basis established in Sec. IV [Eq. (9)], the lack of change of Ni L-edge cross section also implies that the number of

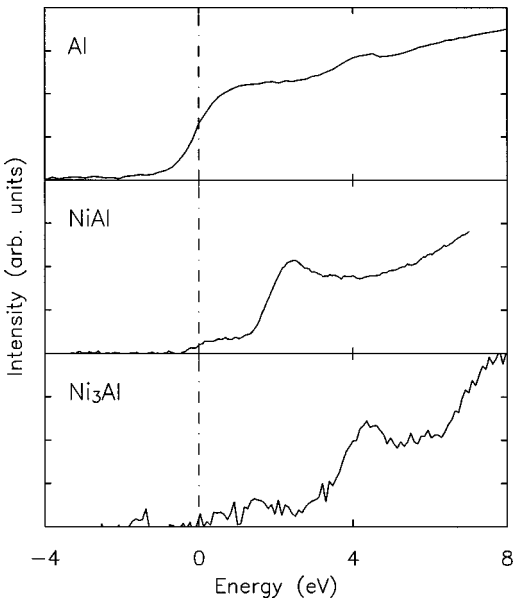

FIG. 7. Measured Al $L_{2,3}$ edge for the $Ni_{1-x}Al_x$ system showing the increase in hybridization ''pseudogap'' at the onset of the L_3 edges with increasing Ni concentration. The spectra are aligned at the edge onset.

LCAO d holes per Ni site also does not change by more than 2% (the experimental uncertainty). In Sec. VI the electronic origins of these trends are considered.

VI. BULK ELECTRONIC STRUCTURE

A. Theoretical approach

The starting point for most modern band-structure calculations is the density-functional theory of Hohenberg and Kohn and Kohn and Sham.[79,80] We briefly review this formulation, to remind readers of the difference between the Kohn-Sham eigenvalues and the quasiparticle excitations of the real system (which we will be measuring). Hohenberg and Kohn[79] showed that the total ground-state energy of a system of interacting electrons (and classical ions) could be written exactly as a functional of the density. The functional is minimal at the true ground-state density and the value of the functional at the minimum is the total energy of the ground state. Kohn and Sham[80] proved that the functional could be minimized by self-consistently solving the one-particle Schrödinger equations

$$[-\tfrac{1}{2}\nabla^2+V_{\rm ext}(\boldsymbol{r})+V_H(\boldsymbol{r})+V_{\rm xc}(\boldsymbol{r})]\psi(\boldsymbol{r})=\epsilon_i\psi(\boldsymbol{r}), \quad (14)$$

where V_H is the Hartree potential, $V_{\rm ext}$ is the classical external electrostatic potential, and $V_{\rm xc}$ is the exchange-correlation potential. The fully interacting many-body problem has been mapped onto a set of self-consistent equations for noninteracting electrons. The theory does not provide a physical meaning for the single-particle eigenvalues ϵ_i and the eigenfunctions $\psi(\boldsymbol{r})$, which are needed only to construct the charge density on which the density-functional theory depends.

The occupied Kohn-Sham eigenvalues are often identified with the energies required to excite electrons, and the unoccupied eigenvalues are identified with the excited single par-

ticles. There is no rigorous justification for doing this, as the actual energies for adding or removing electrons from the system are determined by a *different* Schrödinger-like equation that contains a nonlocal, energy-dependent self-energy in place of the exchange-correlation potential[81]. Formally, the quasiparticle energies are the solutions E of the Schrödinger equation[81]

$$\left[-\frac{1}{2}\nabla^2 + V_{\text{ext}}(\boldsymbol{r}) + V_H(\boldsymbol{r}) + \int \Sigma(\boldsymbol{r},\boldsymbol{r}',E)\,\psi(\boldsymbol{r}')\,d\boldsymbol{r}' \right] \psi(\boldsymbol{r}) = E\,\psi(\boldsymbol{r}). \qquad (15)$$

Whereas the exchange correlation potential, $V_{\text{xc}}(\boldsymbol{r})$ used in the Kohn-Sham equations [Eq. (14)] is both local and independent of energy, the self-energy $\Sigma(\boldsymbol{r},\boldsymbol{r}',E)$ is a nonlocal energy-dependent operator. The eigenstates of this new equation [Eq. (15)] are the energies of the quasiparticles of the system. The quasiparticles are noninteracting particles which move in an effective potential that is nonlocal and energy dependent. The quasiparticle energies are generally complex, reflecting the finite lifetime of excitations in the system. The Kohn-Sham eigenvalues, however, are real. It is necessary to add finite lifetimes to the Kohn-Sham density of states if they are to be compared with measured excitation spectra.

The complicated structure of the self-energy operator makes it very difficult to calculate the quasiparticle spectrum exactly. With the use of the local-density approximation (LDA), the Kohn-Sham equations are considerably easier to solve. Although the Kohn-Sham eigenvalues are not intended to reproduce quasiparticle excitations of the system, the two treatments should yield similar effective single-particle spectra in cases where the many-body effects (from the self-energy or exchange-correlation terms) are slowly varying. Numerous calculations and experiments have shown very good quantitative agreement between LDA electronic structures and experiment in well-hybridized transition metals and compounds like the aluminides discussed here.[82,4,15,16,29]

In metallic systems at zero temperature, the chemical potential (or the Fermi energy) is given by the highest occupied Kohn-Sham eigenvalue.[83] There is no exact relationship away from the Fermi energy. However the difference between the quasiparticle and the LDA eigenvalues is (to first order in $[\Sigma-\Sigma_{\text{LDA}}]$) just the difference in self-energies. Near the Fermi energy, the self-energy in metals is expected to be slowly varying, so the LDA and the quasiparticle DOS will have the same shape. As the excitation energy increases, so do the deviations between the calculated and measured DOS's.[84,85]

In Sec. VI C the excitation spectra measured with EELS are compared to the Kohn-Sham density of states calculated within the local-density approximation using the mean APW method (see Sec. VI B). Good agreement between the measured spectra and the calculated DOS lends credence to the single-particle description of the EELS edges.

B. LAPW band-structure calculations

Self-consistent, full-potential, linear-augmented-plane-wave (LAPW) calculations for Ni, Ni_3Al, NiAl, and Al were performed. The NiAl calculations are very similar to those previously reported.[34] A general description of the method can be found in Singh.[52] Plane waves are used to expand the basis and potentials outside the spheres. Inside the spheres the basis is expanded up to $l=8$, and additional local orbital extensions were used to avoid linearization errors. This is sufficient to ensure good convergence over the energy range of interest, roughly 2 Ry (see Ref. 11). The sphere radii are given in Table II.

TABLE II. Summary of parameters used in the LAPW calculations. (See text for more details on the k-point sets.)

	Lattice constant (a_0)	Sphere radius (a_0)	No.of k points for the charge density	No. of k points for the DOS
Ni	6.650	2.31	408	145
Ni_3Al	6.743	2.38	120	165
NiAl	5.450	2.30	20	165
Al	7.651	2.30	60	413

As the Ni and Al $2p$ core states are well localized inside these spheres, only the muffin tin portion of the wave function is used to calculate the partial DOS and EELS oscillator strengths. The LAPW basis does not satisfy Eq. (10), so the factorization of the LAPW transition matrix elements into a radial matrix element and a LDOS is only approximate. However, as shown in Sec. IV B, it is a very good approximation for core levels.

Spin polarization was only included for the Ni calculation. Although Ni_3Al is thought to be a weak itinerant ferromagnet,[86,87] its Curie temperature of 43 K is well below the measurement temperature ($\approx$300 K). For comparison with experiment, Ni_3Al is assumed to be paramagnetic. Simulations of the magnetic properties of Ni_3Al can be found elsewhere.[13,17–19] The magnetic effects, even at 0 K, are very weak, and the error made in neglecting them ($\approx$0.003 eV) is much smaller than the energy scale of interest in this work ($\approx$0.1 eV).

The ground-state crystal structures and the experimental lattice constants (see Table II) were used. A special k point set[88] was used for the self-consistent calculation of the charge density, while a uniform mesh including the Γ point was used for the DOS. In Ni and Ni_3Al the d band is sharply varying near the Fermi energy, so larger k-point sets were used than for NiAl or Al. In the calculation of the Ni charge density a large k-point set (Table II) was needed to ensure good convergence of the magnetic moment. The number of k points in the irreducible $\frac{1}{48}$th wedge of the Brillouin zone for each of the compounds studied are given in Table II.

1. Results

The total and partial DOS's from the present calculations are shown in Figs. 8–11. The shapes of the DOS's are qualitatively similar to the previously mentioned works,[13,17–19,22] although the fine features of the partial DOS's do sometimes differ. The most noticeable difference is the presence of a small peak in the Ni_3Al Al s DOS at 0 eV (Fig. 10). This is not present in the full-potential linear-muffin-tin orbital (FP-LMTO) calculations of Sun *et al.*[22] We doubled the k-point

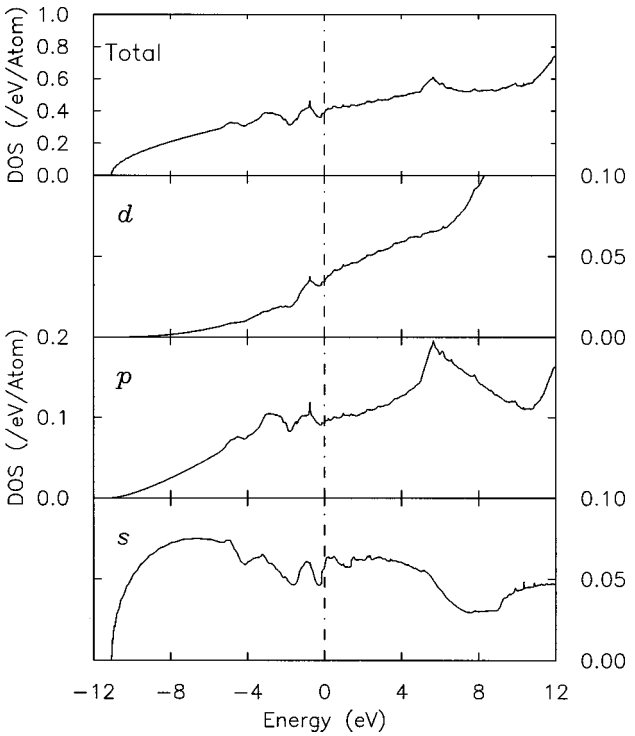

FIG. 8. LAPW calculated density of states for Al. The total DOS for the unit cell is given in the top panel. Below are the DOS's decomposed by angular momentum inside the muffin-tin sphere. The Fermi energy is taken as the zero of the energy axis. Note the resemblance to a free-electron DOS, especially at low energies.

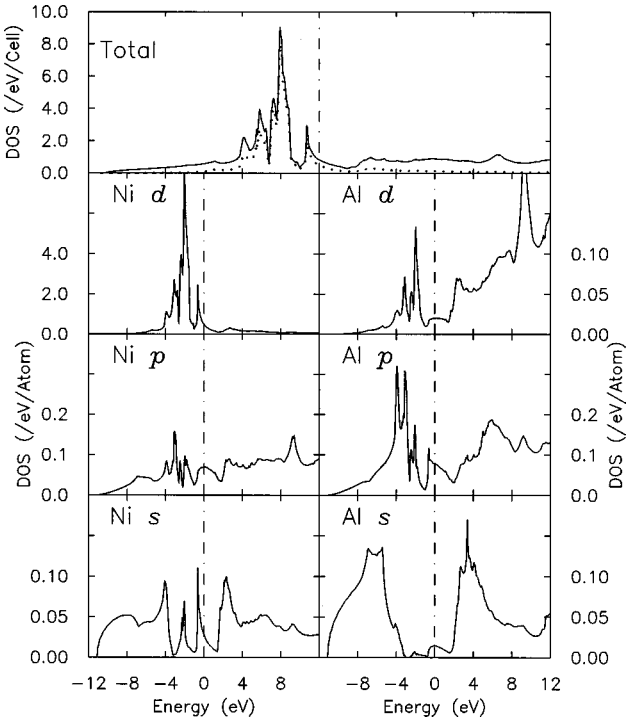

FIG. 9. LAPW calculated density of states for NiAl. The total DOS for the unit cell (solid line) and the Ni *d* DOS (dotted) are given in the top panel (the energy axis is −12 to 12 eV). Below are the DOS's projected onto the Ni and Al spheres.

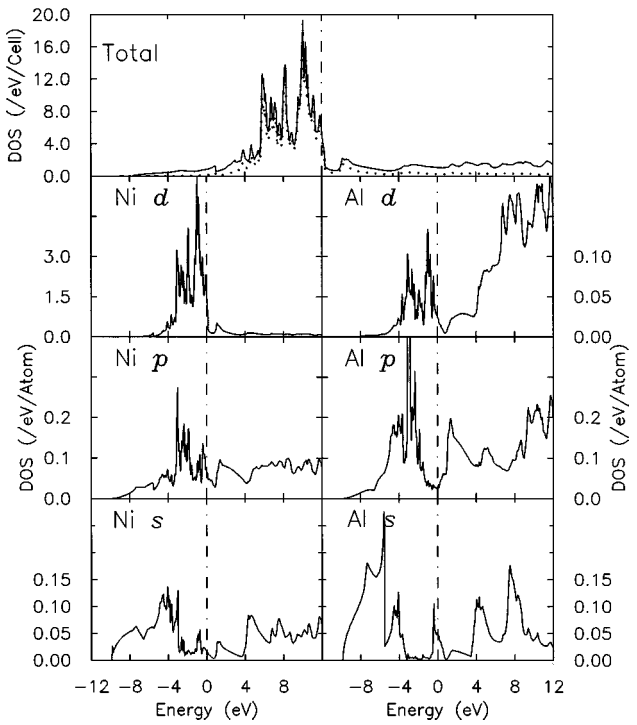

FIG. 10. LAPW calculated density of states for Ni_3Al. The total DOS for the unit cell (solid line) and the Ni *d* DOS (dotted) are given in the top panel (the energy axis is −12 to 12 eV). Below are the DOS projected onto the Ni and Al spheres.

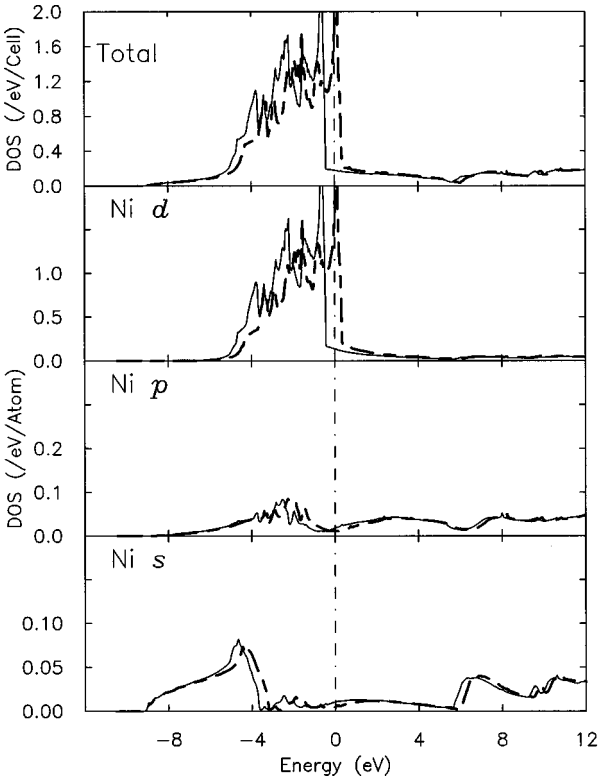

FIG. 11. LAPW calculated density of states for spin-polarized Ni. The majority-spin states are plotted with a solid line and the minority-spin states with a dashed line. Only the central portion of the states (the ''*d* band'') has a large exchange splitting. Notice also the ''scooping out'' of the *s*DOS around the *d* band from the strong *s*-*d* hybridization. The resulting hybridized states have piled up at −4 and +4 eV.

TABLE III. Angular decomposition of the LAPW valence charge in the muffin-tin spheres. I is the charge in the interstitial region (divided by the number of atoms in the unit cell to make comparison between the different compounds easier). Both because of the large interstitial charge and the use of different sphere radii, the changes in muffin-tin charges cannot be directly interpreted as intersite charge transfers.

	Ni s	Ni p	Ni d	Ni f	Al s	Al p	Al d	Al f	I
Ni	0.463	0.446	8.226	0.031	-	-	-	-	0.834
Ni_3Al	0.502	0.508	8.423	0.028	0.706	0.820	0.220	0.039	0.707
NiAl	0.435	0.444	8.378	0.016	0.618	0.759	0.177	0.025	0.574
Al	-	-	-	-	0.676	0.615	0.111	0.006	1.592

set for our LAPW calculations and saw no noticeable changes in the DOS. As we were concerned that the feature may be an artifact of the basis set chosen, we repeated the calculations using Anderson's LMTO-ASA (atomic sphere approximation) method[54] with 286 k points in the irreducible Brillouin zone. This gave a remarkably similar peak, suggesting that it may be a real feature and one worth investigating experimentally with a higher-energy resolution than the 0.8 eV used in this study.

The LAPW Al DOS shown in Fig. 8 is included mainly to emphasize the trends in the Al partial DOS when Al is alloyed with Ni. The overall shape of the Al DOS closely resembles that of a free-electron gas. Although atomic Al has only s and p electrons, the fcc Al crystal has s, p, *and* d projected states. The overall shape of the s, p, and d partial DOS's again resemble the partial DOS of a free-electron gas. The presence of the valence d states in the Al crystal should serve as a warning that states with d symmetry in the solid are not restricted solely to elements that have valence d electrons as free atoms.

The cusps in the Al DOS arising from Van Hove singularities at the zone faces and zone edges[89] are fully reproduced in Fig. 8. The k-point sampling near the zone boundaries would have to be increased to reproduce these features. This is not a serious problem, as the main interest in these calculations is to simulate core excitations where the intrinsic core hole lifetimes broaden the spectra to a greater extent than does the error in the k-point sampling. (A more densely sampled DOS can be found in Szmulowicz and Segall,[90] as well as its comparison to a measured Al K edge.)

2. Bands and bonding trends

In the alloys, the free-electron band is common to both Ni and Al. This is most clearly illustrated in the Ni and Al s DOS's of Fig. 9. Both bands start at the same energy and have the $\sqrt{E}$ dependence typical of a free-electron gas at low energies. However, strong departures from the free-electron model occur for sites that are adjacent to a d resonance. The free-electron states are ''scooped out'' around the resonance, and redistributed to energies above and below the d band. The effect is most pronounced for the Ni s DOS in bulk Ni (which has the most nearest neighbors with d resonances). The mixing is between nearest neighbors, not orbitals on the same site as can be seen by comparing the s DOS for Ni and Al in NiAl (Figs. 9 and 15). In contrast to the above case, the scooping out is more pronounced on the Al site which has eight Ni nearest neighbors, than on the Ni site which has no Ni nearest neighbors. That there is a gap at all on the Ni sites is due to the six Ni next-nearest neighbors which are $\sqrt{2}$ more distant. These trends are best understood in terms of s-d and p-d hybridization (Sec. VIII).

Notice that the Ni d DOS accounts for a large portion of the total DOS's, especially in the Ni-rich compounds. A characteristic feature of the Ni d states is the large, narrow peak in the DOS from roughly 4 eV below the Fermi level to about 1 eV above the Fermi level. These states provide most of the magnetic moment for pure Ni (Fig. 11). It is this narrow portion that is often identified with the width of the d band.[91,16] However, there are also states outside this region which have d symmetry. The LAPW calculations (and the EELS experiments) do not offer any physical arguments that distinguish between states in the peak and states in the broad background (other than perhaps a separation into magnetic and nonmagnetic states). Far from the narrow peak, the d states start to resemble the d states of a free-electron continuum (as discussed above for the case of Al). In a tight-binding calculation, the peaked region is composed largely of Ni 3d states. It is not, however, possible to uniquely separate the LAPW d DOS in to continuum and 3d states as these features become mixed and altered in any real system.

The effects on the analysis of the DOS can be quite pronounced. For instance, Liu *et al.*[16] concluded that the Ni d band in NiAl is narrower than in pure Ni while Carlsson,[36] using a different definition of the Ni d band, found it to be broader in NiAl than in pure Ni. Despite these ambiguities, it is common for experimentalists to divide the measured EEL and XAS spectra in to d holes and a continuum background.[76,91–93,26,25,94,95] The danger in performing such fitting exercises is that they rarely allow for the states to mix or drastically alter their shapes (such as has occurred in the Ni-Al alloys).

3. Charge transfers and oscillator strengths

The valence charge, partitioned by site and angular momentum, is given in Table III. There are no clear trends, other than to note that the charge redistributions rarely exceed 0.1 electron. The total charges in the Ni and Al centered spheres are more sensitive to the sphere size (Ni_3Al has a larger sphere than Ni, Al, or NiAl) than the type of neighboring atoms. As the changes in interstitial charge are much larger than the changes in charge associated with the Ni or Al spheres, these results should not be taken as evidence for an intersite charge transfer.

A discussion of bonding is more easily dealt with using an atomlike basis set (see Sec. III). As mentioned in Sec. IV, an experimentally measurable quantity that is proportional to an

TABLE IV. Angular decomposition of valence oscillator strength. Only the radial portion of the final-state wave function is used. While a good approximation for the Ni *d* states, it leads to large errors for the more delocalized Al wave functions.

	Ni *d*	Al *s*	Al *p*	Al *d*
Ni	7.13	-	-	-
Ni_3Al	7.20	0.196	0.16	0.07
NiAl	7.16	0.180	0.15	0.12
Al	-	0.197	0.12	0.13

atomiclike partial DOS is the EELS oscillator strength. If the oscillator strength [Eq. (6)] integrated up to the Fermi energy is used as a measure of charge, then the charges associated with each site are seen to be very similar (Table IV) in all the systems studied (Ni, Ni_3Al, NiAl, and Al). As discussed in Sec. IV, the oscillator strength provides a measure of charge associated with a particular angular character that is not sensitive to the sphere radius used in the calculation, since only charge density that overlaps with the core wave functions is sampled. This makes the oscillator strength insensitive to charge redistributions that arise from bond formation. Only intersite charge transfers (i.e. from near the Al core to near the Ni core) can alter the oscillator strength. This is less than 2% for the Ni *d* DOS in bulk Ni vs NiAl.

A similar analysis can be made for the unoccupied states. The oscillator strength, integrated from the Fermi energy to 14 eV above the Fermi energy, measures a quantity roughly proportional to the experimentally determined EELS cross sections of Table I. The experimental data is integrated from the Fermi energy to 35 eV above the L_3-edge onset, so as to include the L_2 edge as well. As a result of the (small) spin-orbit couplings in the real system, both L_2 and L_3 edges have to be summed over to give equal weighting to all the final states.[96,97] The states are already equally weighted in the calculations, so a smaller window of integration can be used. The integrated oscillator strengths are 2.03, 1.99, and 2.03 for Ni, Ni_3Al, and NiAl, respectively. The relative changes in the oscillator strength (as in the experimental data) are less than 2%. This also implies that the number of holes of *d* character (per Ni atom) also does not change by more than 2% upon alloying Ni with Al.

C. Comparison of theory and experiment

So far the core hole and the excited electron have been assumed to have infinite lifetimes. The core hole can decay by x-ray or Auger transitions, and the excited electron can lose energy by emitting electron-hole pairs and drop to the Fermi level. These lifetimes broaden the initial and final states. The treatment of the lifetime effects closely follows that of Müller and Wilkins,[4] and are described in Appendix C, as are corrections for the instrumental resolution. The measured EELS spectra follow the broadened, calculated ground-state *d* DOS (Fig. 12). If the spectra are normalized at threshold then there is a roughly 10% discrepancy between the two at higher energies. For Ni, the calculated oscillator strength is too large, while for Ni_3Al and NiAl it is too small for $E>8$ eV. There are also some small but systematic discrepancies in the position of features away from E_F; the

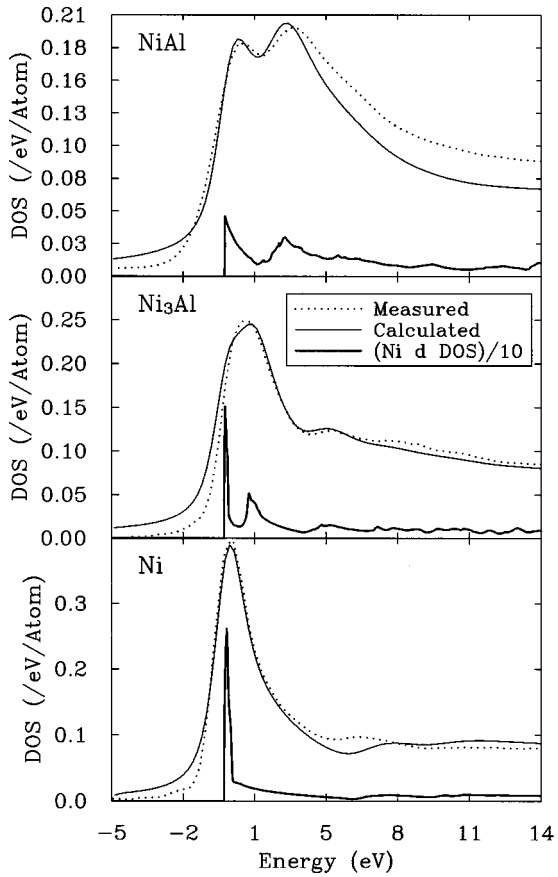

FIG. 12. Comparison of the LAPW calculated and measured Ni L_3 EELS edges for the $Ni_{1-x}Al_x$ system. The oscillator strength (dark solid line) is calculated directly from Eq. (6). Lifetime broadening of the calculation (light solid line) is described in Appendix C.

energy splitting between the first and second peaks in the NiAl spectrum is 10% greater in the experiment than the calculation. The zone-boundary divergence (the steplike feature) in the DOS at 7 eV above the Fermi level in the Ni calculation[24,3,98,84] appears at 6 eV above the Fermi level in the measurement.

The agreement between the measured EELS spectra (which probe excited states) and the calculations (which are approximations to the ground states of the different alloys) is quite good. All of the features in the experiment can be found in the calculation, if slightly stretched or altered in intensity. The largest discrepancies are for the Al *L* edge in Ni_3Al. This is the weakest signal of the Al *L* edges studied, and where the uncertainties in the shape of the background due to the Ni *M* edge are largest. However, even accounting for possible contributions from the background, the peak at 4 eV in the experiment is sharper than in the calculation. This may be due to the limited *k*-point set used in the calculation. Most of the other discrepancies can be attributed more to the LAPW and local-density approximations rather than to core-hole effects. For instance, the zone boundary at 6 eV in the Ni EELS measurement is also found at 6 eV in the bremsstrahlung isochromat spectrum, where there is no core hole.[91] However the position of this steplike feature (identified as a L_1,K_2 critical point by Szmulowicz and Pease[24]) varies from calculation to calculation.[24,3,98,84]

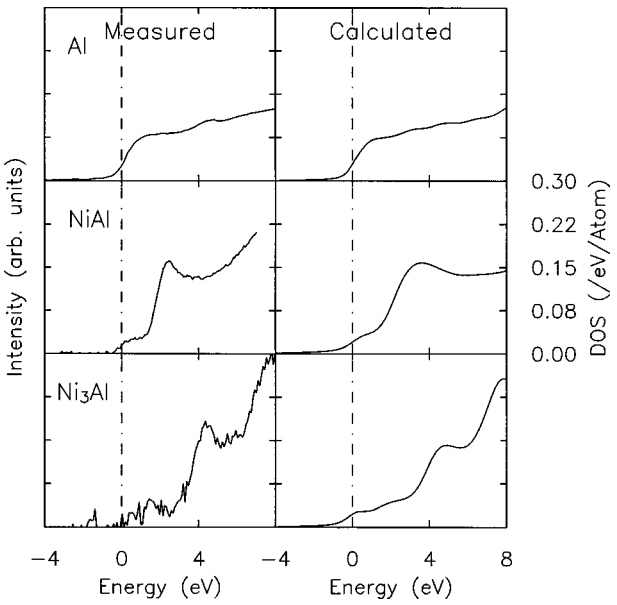

FIG. 13. Comparison of the LAPW calculated and measured Al $L_{2,3}$ EELS edges for the $Ni_{1-x}Al_x$ system.

The trends in the calculated Al L edge closely follow those measured with EELS (Fig. 13). A more quantitative comparison cannot be made due to the errors in the background subtraction of the experimental data. Nevertheless, the formation of a pseudogap and the subsequent scooping out of the Al DOS away from energies of the Ni d band are seen in both theory and experiment.

The formation of pseudogaps in the s and p states, where they cross the d band, is a central motif in the Ni-Al system (good experimental examples can be found in Sarma *et al.*[15] and Liu *et al.*[16]). The reduced density of states can be understood in terms of s-d mixing (or hybridization), which scoops states away from those energies where the bands cross. The importance of these gaps in the alloying of transition metals with free-electron-like elements was emphasized in Refs. 38 and 99. These trends in the local densities of states are well suited to a moments-based analysis.[100] In particular, formation of the pseudogap can be understood in terms of changes of the fourth moment of the s DOS. A similar effect for the d DOS is also observed experimentally, and was previously discussed by Carlsson[36] for the Ni-Al system. The bond-order potentials of Pettifor and co-workers,[101,39,102] Aoki,[40] and Horsfield *et al.*[41] provide a qualitative framework for connecting changes in the local moments to changes in cohesive energy. In Sec. VII we review this in a formalism suitable for the analysis of the EELS spectra.

VII. REAL-SPACE MODELS OF ELECTRONIC STRUCTURE

Ab initio calculations have revealed some important trends in the bulk alloys, and have shown that the measured EELS spectra can be accurately modeled with the LDA DOS. This match so far is only a fingerprinting (i.e., a match of the EELS fine structure). What is still needed is a model that relates the changes in the measured LDOS at grain boundaries (such as in Muller *et al.*[1]) and defects to the altered local mechanical properties.

Often the changes in the EELS spectra of alloys are explained in terms of a rigid-band picture.[94,10] It is assumed that the shape of the bands (and hence the local DOS) do not change upon alloying. Instead, only the Fermi level is allowed to vary as the superimposed densities of states are filled with the electrons from the constituent atoms. For instance, the decrease in the height of sharp peak at the onset of the Ni L edge as Al is added to the system would be described as a charge transfer from Al to Ni, filling the Ni d band. There are some problems with this interpretation. First, the total area under the measured Ni L edge [as defined by Eq. (B2)] does *not* change appreciably upon alloying (Table I). Second, as seen in Secs. V and VI, the shapes of the local DOS change considerably upon alloying, whereas, in the rigid-band picture, the shapes of the local DOS are assumed to remain fixed and only the filling of the DOS is allowed to vary. Further, the assumed charge transfers on which the rigid-band picture is based, makes it very difficult to give any quantitative predictions for the heat of formation of the alloys.

Instead, this section describes an alternative approach, based on modern tight-binding theory, which overcomes these obstacles. The moments of the LDOS may be determined from the geometry of the lattice, which is a real-space description that treats crystals and defects on an equal footing. In Sec. VII A this procedure will be used to connect the shape changes in the measured EELS spectra to changes in the local geometry, as well as to simple rules for ordering trends and alloy heats of formation. The connection between EELS measurements and cohesive energies was given in companion papers.[42,97]

Linking changes in the local densities of states to changes in cohesive energy can be done with the use of the ''force theorem'' of Pettifor[103] and Mackintosh and Anderson.[104] This states that given a self-consistent solution to the Kohn-Sham equations, the first-order change in total energy δE is given by

$$\delta E = \delta\left(\sum_i n_i \epsilon_i \right) + \delta E_{\rm es}. \tag{16}$$

The first term is the change in the occupied one-electron states of energy ϵ_i and occupancy n_i, calculated using the displaced (by the perturbation) but otherwise frozen one-electron potential. $\delta E_{\rm es}$ is the change in the classical electrostatic energy. If the cell defining the perturbed atom were neutral and spherically symmetric, then $\delta E_{\rm es}$ would be zero. Otherwise it would be the change in the Madelung energy. When choosing to work with a charge neutral system, a first-order *change* in the total energy is given simply by the change in the Kohn-Sham single-particle eigenvalues. (Even though the total energy itself is not given by the eigenvalue sum). The key result of the force theorem is that the double counting terms in the Coulomb energy have been canceled out. Although these exchange and correlation energies do make an important contribution to the total energy of the solid, they do not contribute to a first-order change in the total energy.

The first term of Eq. (16) can be rewritten as $E_{\rm bond}+E_{\rm prom}$. The promotion energy $E_{\rm prom}=\Sigma_i \delta n_i \epsilon_i$ takes into account the change in occupancy of the orbitals on forming the solid from the reference system. If the reference system is chosen as the free atom with orbitals at energies $\{\epsilon_I\}$, then the bond energy, $E_{\rm bond}=\Sigma_i n_i \delta\epsilon_i$ can be rewritten, using Eq. (2), as

$$E_{\rm bond}=\sum_I \int_{-\infty}^{E_F}(E-\epsilon_I)n_I(E)dE, \tag{17}$$

where $n_I(E)$ is the I-projected LDOS and E_F is the Fermi energy (for simplicity only metals at $T=0$ K are considered—a Fermi function must be introduced at finite temperatures). This describes the covalent bonding that occurs when the solid is formed from the free atoms. States lower in energy than those of the free atom are termed bonding states. States at higher energies than the free atom are antibonding. This is reflected in Eq. (17), which changes sign at $E=\epsilon_I$.

If the charge transfers upon alloying are negligible (as the EELS measurements suggest for the Ni-Al system) then the bond energy $E_{\rm bond}$ is the dominant contribution to the change in cohesive energy. As a caveat, this approximation is most appropriate for normal metals, and is expected to break down in ionic materials where the electrostatic contributions are important, or strongly correlated systems where higher-order terms such as changes in the exchange and correlation energies become comparable to changes in the bond energy.

The force theorem explains the success of tight binding and molecular-orbital theory in predicting structures and heats of formation from eigenvalue sums, when the sums themselves are not good models of the total energy. For this work, the relevant feature of the force theorem is that changes in the bond energy are directly related to changes in the local density of states [through Eq. (17)].

A. Moments theorem

The link between the shape of the electronic density of states and the local arrangement of atoms in a solid is provided by the moments theorem of Cyrot-Lackmann.[100,105] As we will be using the results of the theorem for analysis, not calculations, it will be stated in its simplest form, assuming an orthogonal basis of atomic orbitals $|I\rangle$, where $I=i\alpha$ labels both the site and the orbital. (Using Anderson's chemical pseudopotential theory, such a basis can always be constructed,[106] although it need not be unique or particularly transferable.) The local density of states associated with I is

$$n_I(E)=\sum_k |\langle I|k\rangle|^2 \delta(E-E_k), \tag{18}$$

where $k=\{n,\vec{k}\}$ labels the eigenstates with eigenvalues E_k. The diagonal matrix elements of the Hamiltonian in the atomic basis are $\langle I|H|I\rangle=H_{II}=\epsilon_I$. These are used as the reference energies for calculating the pth moment of the local density of states:

$$\mu_I^{(p)}=\int_{-\infty}^{\infty}(E-\epsilon_I)^p n_I(E)dE. \tag{19}$$

The key result of the moments theorem was to show that the pth moment of the LDOS on site I can be calculated locally, without knowledge of the eigenvalues of the entire system, as

$$\mu_I^{(p)}=\langle I|(H-\epsilon_I)^p|I\rangle=[(H-\epsilon_I)^p]_{II}. \tag{20}$$

Expanding the powers of p should make this more apparent:

$$\mu_I^{(p)}=\sum_{I_1,I_2,\cdots,I_{p-1}}[(H-\epsilon_I)]_{I,I_1} \times[(H-\epsilon_I)]_{I_1,I_2}\cdots[(H-\epsilon_I)]_{I_{p-1},I}. \tag{21}$$

This links the moments of the local densities of states to the local geometry through all the hopping paths of length p which start and end on the same site. As a consequence, atoms that are more than $p/2-1$ hops away from site I cannot affect the lowest p moments of the LDOS on site I.

The lower moments have simple physical interpretations. The zeroth moment $\mu_I^{(0)}=1$ as there is only one orbital per label I. The first moment is the average energy measured with respect to the center of the band, which is always 0:

$$\mu_I^{(1)}=[(H-\epsilon_I)]_{I,I}=H_{I,I}-\epsilon_I\delta_{I,I}=0. \tag{22}$$

The expression for $\mu_I^{(2)}$ can be simplified by noting that unless $I'=I''$, $[(H-\epsilon_I)]_{I',I''}=H_{I',I''}$. This means the second moment can be written as

$$\mu_I^{(2)}=\sum_{I_1\neq I}|H_{I,I_1}|^2, \tag{23}$$

where H_{I,I_1} is the nearest-neighbor hopping integral which is a function of the distance between sites I and I_1 (see Harrison[107] for analytic models of H_{I,I_1}). The second moment is by definition the variance (the mean-square width) of the local density of states, so Eq. (23) shows *the width of the LDOS on a given atom is determined only by its nearest neighbors*. (For a monoatomic material, the width of the LDOS will vary as the square root of the number of nearest neighbors.[100,105,44])

The second moment is a natural unit of measure for the energy scale, and allows us to express the higher moments as dimensionless quantities. It is these higher moments that determine the *shape* of the LDOS. The dimensionless third and fourth moments are $\gamma_3=\mu_I^{(3)}/(\mu_I^{(2)})^{3/2}$ and $\gamma_4=\mu_I^{(3)}/(\mu_I^{(2)})^2$, respectively. The third-moment determines the skewness of the DOS, and the fourth moment determines whether the DOS is bimodal or unimodal. The exact measure of the kurtosis is determined by the parameter

$$s=\gamma_4-\gamma_3. \tag{24}$$

A large parameter ($s>1$) implies a single peak, while a small parameter implies that the spectrum has separated into two peaks. We will refer to s as the normalized fourth moment. Worked examples of the calculation of the higher moments can be found in Sutton.[46]

The connection between the local moments of a DOS and the contribution of that DOS to the bond energy can be made by expanding the bond integral of Eq. (17) into the bond-order potentials developed by Aoki[40] and Pettifor.[102] Rather

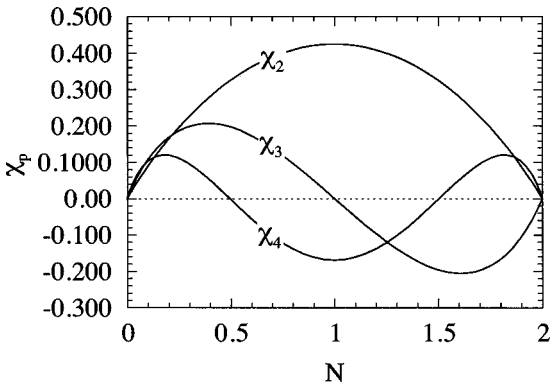

FIG. 14. The reduced susceptibilities χ_p as a function of the number of electrons per orbital, N. χ_p gives the pth moment contribution to the bond energy. χ_p was calculated in the ring approximation (Ref. 39).

than expressing the bond energy in terms of the local density of states as in Eq. (17), Aoki showed that the bond energy can be expanded directly in terms of the local moments as

$$E_{\mathrm{bond},I} = -d_l\sqrt{\mu^{(2)}}[\chi_2(N)+\chi_3(N)\gamma_3+\chi_4(N)(s-2) + \cdots], \tag{25}$$

where l is the orbital quantum number and the degeneracy $d_l=2(2l+1)$. The leading factor of 2 is from the assumed spin degeneracy.

The reduced susceptibilities χ_p are essentially functions only of the number of electrons per orbital, N. A general feature of the susceptibilities is that χ_p changes sign $p-1$ times as the band is filled. Figure 14 shows χ_p calculated in the ring approximation.[39]

The separation of the bond energy into contributions from band filling (χ_p) and local geometry (the moments) simplifies the discussion as it makes clear the difference between the effects of charge transfers (changes in N) and rehybridization (changes in the moments). The results of Table I suggest we should assume local charge neutrality for the Ni d states when alloying with Al. This implies that χ_p for Ni does not change much upon alloying with Al and is determined essentially by the number of electrons per orbital of the pure metals. The changes in the bond energy then result from changes in the local moments, which do change on alloying (as they depend on the local geometry and composition). Thus Eq. (25) provides an explicit link between local changes in bond energy, electronic structure, and geometry.

B. Fourth moment and the hybridization pseudogap

Knowledge of the second moment alone is not sufficient to explain the behavior of the Ni and Al L edges upon alloying. Not only do the bandwidths change (which is a second-moment effect), but the shape of the edges also change (and shape changes are determined by the higher moments). This is particularly apparent for the Al L edge series (Fig. 13) where a pseudogap grows with increasing Ni concentration. The formation of the pseudogap splits the Al DOS into two peaks, and this is essentially an effect described by changes in the fourth moment. In part, the failure of the second moment to describe the bonding trend is because the second moment contains no information about the angular interactions or the directionality of the bonding.[36,108,109] (Three points are needed to define an angle, and only two are provided in the evaluation of contributions to the second moment.)

The angular character of the bonding is important because the pseudogap is the result of s-d hybridization. In a traditional bandstructure description,[110,35] this can be understood in two steps. First, the narrow d band is crossed by the broad free-electron-like s band. Second, where the bands cross, the s and d states interact and mix (hybridize). As we might expect from second-order perturbation theory (or by diagonalizing the Hamiltonian), the mixed states lie above and below the original crossing. In other words, states are scooped out from the point where the bands would have crossed, reducing the DOS and leading to the pseudogap. A good example of this hybridization in NiAl can be found in Liu *et al.*[16]

The same effect also has a very simple explanation in terms of the local moments. The scooping out that is seen to occur during s-d hybridization is essentially a fourth-moment contribution. This is particularly important as Carlsson[36] found the fourth-moment contribution to the heat of formation of a transition-metal–aluminum alloy to be comparable to the second-moment term. He explained that the increase in the fourth moment of the d DOS as a transition metal is alloyed with Al can be understood as follows: The rapid angular variation of d-d hopping matrix elements leads to a phase cancellation in the normalized fourth moment γ_4, calculated in a pure transition metal (a graphical example of the rapid oscillation of γ_4 with bond angle can be found in Moriarty[108]). The s-s hopping parameters have no angular variation, so systems with predominantly s electrons will have much larger fourth moments ($\gamma_4\approx 4$). In the limit of a d-electron impurity embedded in a free-electron gas, the d DOS has a Lorentzian profile ($\gamma_4\approx 4$) while a pure transition metal has a roughly rectangular d DOS ($\gamma_4=2$). This suggests that the energy gain with the extent of hybridization is smoothly varying as γ_4 increases from 2 to 4.

That the energy change is a smoothly varying function of γ_4 (and hence s), is expected from Eq. (25). A larger fourth moment places more states in the tails of the distribution, and this gives a lower bond energy for nearly empty and nearly full bands. The trend from a close-packed structure to a bcc structure and back to a close-packed structure across the transition-metal series can be explained by the difference in the fourth moment between a bcc and a close-packed (fcc or hcp) structure.[111]

Returning to the Ni-Al alloys, as more Ni nearest neighbors are placed around an Al atom, the increased phase cancellation (from replacing s by d states) will result in a reduced fourth moment. The reduced fourth moment on the Al sites after alloying with Ni makes the Al DOS more bimodal (i.e. splits it into two peaks)—this is the ''scooping out'' due to the s-d hybridization expressed in real-space terms. The trend is best illustrated by examining the calculated s DOS for the Ni-Al alloys (Fig. 15). The size of the gap increases with the number of neighboring Ni atoms. The same dependence of the fourth moment on the number of Ni atoms also determines the shape of the Ni L edges (which measure the Ni d states). The central peak in the Ni d DOS changed from

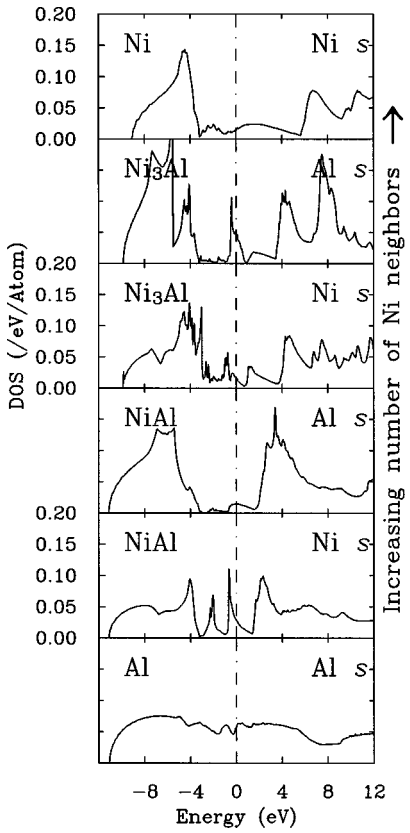

FIG. 15. *s* partial DOS for the $Ni_{1-x}Al_x$ system showing the increase in hybridization ''pseudogap'' with increasing Ni concentration. Both the Ni and Al *s* DOS's are shown. Note that the size of the gap is more strongly affected by the number of neighboring Ni atoms, whether the central atom is Ni or Al.

a rectangular to a Lorentzian shape as the compounds became increasingly Al rich. This results in an increased fourth moment for the Ni *d* states. As the Ni *L* edge is comprised mainly of the tails of the Ni *d* states, and an increase in the fourth moment moves states from the central peak to the tails of the distribution, the more Al neighbors around a Ni site, the more tails are added to the Ni *d* DOS. Consequently the Ni *L* edge loses intensity at the edge onset and changes from a sharp to a broad peak (Fig. 5). This is a real-space argument, as the fourth moment can be calculated from the local geometry, and applies equally well at grain boundaries as in perfect crystals.

Cohesive energy and fourth-moment trends

The trends in the heats of formation of transition-metal–aluminum alloys can also be understood in terms of the moments of the local DOS. The connection follows from Aoki and Pettifor's expansion of the bond energy in terms of the local moments. As with the shapes of the LDOS, the dominant contribution to the bond energy in the Ni-Al system is provided by the fourth moment. The bond energy term is proportional to both the fourth moment $\mu^{(4)}$, and a function χ_4 which is determined essentially by the number of electrons per orbital (and are fixed by charge neutrality in the model).

When more Al nearest neighbors are placed around a Ni atom, the fourth moment of the Ni *d* DOS must increase. As the Ni *d* DOS is almost full, $\chi_4>0$, and this implies that the bond energy per Ni atom is increased (Fig. 14). For a metal with a half-filled *d* band (such as Fe), $\chi_4<0$, and this will result in a bond energy decrease. As more Ni nearest neighbors are placed around an Al atom, the increased directionality of the bonding (*s*-*d* instead of *s*-*s* or *s*-*p*) will result in a reduced fourth moment for the Al site. However, the *s* and *p* states on the Al atom are roughly half-filled, so $\chi_4<0$, and this will increase the cohesive energy. In short, there is always a bond energy gain for Al when alloyed with a transition metal, but the energy change for the transition metals depends on the band filling. The overall bond energy gain will be less for metals in the middle of the transition series than at either end. This explains the large heat of formations for the Ni,Co and Ti alloys with Al and the small heats of formation for Fe-Al alloys. The ordering trends also follow. Ni-Al and Co-Al should be strongly ordered (there is a large *d* DOS fourth moment when Ni and Al are nearest neighbors) but a large *d* DOS fourth moment (which results from Fe-Al nearest neighbors) is energetically unfavorable for the Fe atoms, so the Fe-Al alloys are not as strongly ordered.

VIII. DISCUSSION

The bulk EELS spectra from a series of increasingly Al-rich Ni-Al compounds were examined and the following experimental trends were observed: The Al *L* edge develops a pronounced scooping out in intensity at the edge onset as the compounds become increasingly Ni rich. The Ni *L* edge became increasingly broader and flatter as the Al concentration is increased.

The LAPW calculations of the local densities of states were able to match quite well the measured EELS spectra for bulk Ni, Ni_3Al, NiAl, and Al at an energy resolution of 0.8 eV. This suggests that, for these materials, a single-particle description of the EELS spectra is appropriate, and that core-hole effects (which are not included in the LAPW calculations) are minimal. The success (or the failure) of the single-particle picture relies on two approximations to the many-body treatment (in this case density-functional theory): First, the excitation spectrum of the system should resemble the quasiparticle density of states (for DFT, this is generally true only near the edge onset). This assumes that core-hole excitonic and polarization effects are screened out, conditions that are most readily satisfied for metals to the right of the periodic table. Second, in order to connect the LDOS to cohesive energy trends, the changes in the electron density with respect to some reference system are assumed to be small. When this holds, Anderson's force theorem states that the changes in the total energy are given predominantly by changes in the single-particle eigenvalues, and the remaining many-body effects enter as higher-order corrections. These corrections are important in strongly correlated systems. In ionic systems, the bond energies are smaller than the electrostatic energies, and again, the single-particle picture is not complete.

The trends observed in the measured EELS spectra were reproduced in the LAPW calculations: (i) The scooping out of states at the onset of the Al *L* edge in the Ni-Al alloys is seen more clearly in the Al partial DOS where both the occupied and unoccupied states can be studied. A similar trend

was noted for the Ni *s* DOS. As a general rule, the effect was stronger when the studied site had more Ni nearest neighbors. (ii) The central peak in the Ni *d* DOS changed from a rectangular to a Lorentzian shape as the compounds became increasingly Al rich. Trends (i) and (ii) can be summarized by noting that *increasing (decreasing) the number of Ni atoms surrounding a given site increases (decreases) the fourth moment of the local density of states*. (iii) The calculated EELS oscillator strengths, when integrated over either the valence band or the unoccupied states (0–14 eV above the Fermi energy), also did not change by more than 2% for the *d* states in Ni, Ni_3Al, and NiAl. As discussed in Sec. IV, the oscillator strength provides a measure of charge which is not sensitive to the sphere radius used in the calculation. Only intersite charge transfers (i.e., from near the Al core to near the Ni core) can alter the oscillator strength. This transfer is less than 2% for the Ni *d* DOS in bulk Ni vs NiAl when measured using the oscillator strength (which is proportional to a LCAO basis).

Direct comparison with tight-binding calculations is difficult because a complete basis is never used in calculations, but is implied by the interpretation of the oscillator strength as a LDOS. In other words, the EEL spectrum would contain not only the 3d minimal basis of the calculation, but every state with $l=2$ symmetry. As a result we cannot answer such questions as ''How many $3d$ electrons are there?'' We can, however, make an order of magnitude estimate of this quantity by comparison with the spectrum of Ni in a well-defined atomic configuration, where the $3d$ states can be separated from the $l=2$ continuum. The spectrum of NiO roughly resembles that of a Ni atom in a d^8 configuration. Normalizing the NiO L edge in the same manner as was done for the alloys, the area roughly corresponding to the two $3d$ holes is 138 ± 5 b. Compared to the alloy cross sections given in Table I, this crude estimate suggests that changes in the number of Ni *d* electrons from bulk Ni to the alloys is on the order of 0.1 ± 0.15 electrons/atom.

The single-particle discussion of Sec. VII gave a transparent explanation of the shape changes in the LDOS and related the shape changes to changes in cohesion. The key to both effects was the moments theorem, which relates the moments of the local densities of state to the geometry of the system. The shapes of the Al and Ni DOS in the Ni-Al alloys follow from changes in the fourth moment of the LDOS. The reduced fourth moment on the Al sites with increasing Ni concentration makes the DOS more bimodal—this is the scooping out due to the *s*-*d* hybridization expressed in real-space terms. The trend [number (ii) above] in the Ni *d* DOS is, by definition, also an increase in the fourth moment, which occurs as the number of neighboring Ni atoms is reduced.

The moments-based analysis also provides a simple interpretation of the changes in the ''white line'' (the sharp peak) at the onset of the *L* edge in transition metals. In a tight-binding calculation, the *d* band consists of a narrow central peak with broad tails. It is the unoccupied portion of this narrow central peak which gives rise to the white line in the Ni *L*edges. The white line can be thought of as resulting from the ''unhybridized'' *d* electrons which form only *d*-*d* bonds. Strong *s*-*d* hybridization increases the fourth moment of the Ni *d* DOS, removing *d* states from the narrow *d* band and mixing them with the broader free-electron-like band. At the same time, the central portion of the the *d* band is deformed from a narrow rectangle to a more rounded central peak with tails. This trend can be seen in the progression from Ni to NiAl, where the area in the central peak, relative to the tails of the peak, is a measure of the fourth moment. Strong hybridization implies a larger fourth moment and hence more area in the tails of the distribution and consequently less area in the central peak. As the white line area is the empty portion of the central peak, the smaller the white line, the larger the fourth moment and hence the larger the hybridization energy. This is a very different picture from that suggested by Pearson and co-workers[93,94] where the changes in the white line areas are interpreted as charge transfers.

The interaction of the transition metal *d* states with the more free-electron-like states on neighboring atoms was found to be central to an understanding of the Ni-Al alloys. This should also be true of a wider range of transition-metal–aluminum and silicon alloys. Electronic structure calculations for many of these alloys exist, but experimental studies (especially of defects and boundaries) are still scarce.

IX. SUMMARY

We have described the conditions necessary to relate EELS spectra to calculated, electronic local densities of states (Sec. IV A). By comparison to *ab initio* LAPW calculations for a wide range of Ni-Al compounds, we find the Ni and Al *L* edges closely resemble the ground-state local densities of states, partitioned by site, angular momentum, and chemical species. While there is wide range of choices for local densities of states in a calculation, the EELS oscillator strength selects a unique basis set, which is also proportional to a linear combination of atomiclike orbitals. Interpreting the Ni *L*-edge oscillator strengths using such a basis set, we find, within experimental error, no measurable charge transfers involving the Ni *d* states. Instead the pronounced shape changes seen in the EELS fine structure can be understood in terms of hybridization (mixing) between the narrow *d*-like states at the Ni sites and the more free-electron like states on surrounding atoms. Cyrot-Lackmann's moments theorem proved a useful tool, offering a predictive, real-space analysis of the changes in the EELS spectra. Both the scooping out of states at the onset of the Al *L* edge and the broadening of the sharp peak at the onset of the Ni *L* edge could be understood as changes in the fourth moments of the Ni and Al LDOS's. These changes can be linked to alloy heats of formation and ordering trends with the use of the Force theorem and bond-order potentials. The close links observed between the EELS spectra and the results of a tight-binding bond model will be exploited in a following paper, to obtain quantitative estimates of cohesive energy differences from EEL spectra.[42]

ACKNOWLEDGMENTS

This research was funded by DOE Grant No. DE-FG02-87ER45322. The use of the electron microscopy and materials preparation facilities of the Materials Science Center which is supported by the NSF is acknowledged. The Cor-

nell UHV STEM was acquired through the NSF (Grant No. DMR-8314255) and is operated by the Cornell Materials Science Center (Grant No. DMR-9121654). Support from E. Kirkland and M. Thomas is also acknowledged. The Ni_3Al and NiAl specimens were provided by Shanthi Subramanian and Alice Wu. We thank Professor P. Rez (ASU) for providing us with his Hartree-Slater cross section of the Ni L edge.

APPENDIX A: FACTORIZATION OF THE OSCILLATOR STRENGTH

The separation of the oscillator strength in to a LDOS and transmission function (which is ideally free from environmental effects) cannot be made for an arbitrary choice of basis set. A general derivation and conditions for relating a LDOS to the oscillator strength are given here. We start with the general definition of a LDOS projected on to a basis set $\{|\phi_{i,k,J}(E)\rangle\}$ that depends on energy (E), angular momentum J, the site in the unit cell (i), and some other parameter k (which might represent a quantity such as the crystal momentum):

$$d_{i,J}(E)=\sum_{k,f}|\langle\phi_{i,k,J}(E)|f\rangle|^2\delta(E-E_f). \tag{A1}$$

We now attempt to relate this LDOS to the oscillator strength defined by Eq. (6):

$$F(E)=\frac{1}{3}\frac{2m}{\hbar^2}E\sum_{c,f}|\langle f|r|\phi_c\rangle|^2\delta(E-E_f+E_c). \tag{A2}$$

In comparing the oscillator strength with the LDOS, we must shift the origin by the core-level binding energy E_c. To emphasize the similarity in information, we define $\Delta E_f\equiv E_f-E_c$. As the core states, ϕ_c, are far more localized than the valence states, the basis $\{|\phi_{i,k}(E)\rangle\}$ is assumed to be complete with respect to the core states, i.e.,

$$\sum_{\text{all}i,E,k}|\phi_{i,k}(E)\rangle\langle\phi_{i,k}(E)|=\mathbf{1}. \tag{A3}$$

Substituting this identity into Eq. (A2) gives

$$F(E)=\frac{1}{3}\frac{2m}{\hbar^2}E\sum_f\delta(E-\Delta E_f)\times\left|\sum_k\langle\phi_c|\vec{r}|\phi_{i,k,J}(E_f)\rangle\langle\phi_{i,k,J}(E_f)|f\rangle\right|^2. \tag{A4}$$

Further progress can only be made for the special case that the shape of the wave function has no k dependence; otherwise there will be cross-terms of the form $\langle f|\phi_k\rangle\langle\phi_{k'}|f\rangle$. This implies that the basis set must be factorizable as

$$|\phi_k(E)\rangle=c_k|\phi(E)\rangle. \tag{A5}$$

(The labels i and J have been omitted for clarity.) If the k-independent portion is normalized as $\langle\phi(E)|\phi(E)\rangle=\langle\phi_k(E)|\phi_k(E)\rangle$, then $c_kc_k^*=1$, and c_k only introduces a phase shift. Equation (A5) only need be satisfied in the region of the core orbital.

If the core orbital is localized near the nucleus (as for deep core levels such as the Ni $2p$ state) then the important boundary conditions are the atomic ones, such as the radial wave function vanishing at the nucleus or orthogonality to the core levels. Then the shape of the wave function is determined only by the energy (and the electron density) so Eq. (A5) can be a good approximation in practice.

If, and only if, Eq. (A5) is satisfied (or approximated) then Eq. (A4) can be rewritten as

$$F(E)=\frac{1}{3}\frac{2m}{\hbar^2}E\sum_f|\langle\phi_c|\vec{r}|\phi(E_f)\rangle|^2|\langle\phi(E_f)|f\rangle|^2\times\delta(E-\Delta E_f), \tag{A6}$$

since $c_kc_k^*=1$. This expression is nonzero only for $E_f=E+E_c$, so the first term can be taken outside the summation as

$$F(E)=\frac{1}{3}\frac{2m}{\hbar^2}E|\langle\phi_c|\vec{r}|\phi(E+E_c)\rangle|^2\times\sum_f|\langle\phi(E_f)|f\rangle|^2\delta(E-\Delta E_f). \tag{A7}$$

Equation (A7) has factored the transition terms into an atomlike term and a LDOS. The atomic term is

$$T(E)=\frac{1}{3}\frac{2m}{\hbar^2}E|\langle\phi_{i,c}|\vec{r}|\phi_{i,J}(E+E_c)\rangle|^2 \tag{A8}$$

(the labels i,J have been reintroduced). The second term of Eq. (A7) can be recognized as the LDOS defined in Eq. (A1). These definitions should make explicit the transformation between the EELS oscillator strength and a LDOS whose basis satisfies Eq. (A5),

$$F(E)=T(E)d_{i,J}(E), \tag{A9}$$

which is the desired result.

APPENDIX B: NORMALIZATION OF THE NI L EDGES TO ATOMIC CROSS SECTIONS

The uncertainties in film thickness and calibrating the efficiency of the detector make it very difficult to make accurate measurements of the cross sections on an absolute scale. However, as pointed out by Müller and Wilkins,[4] well above the edge onset where the fine structure is damped out, the overall magnitude of a particular transition (e.g., the Ni L edge) is determined by its corresponding atomic transition (as the extended fine structure oscillates about the atomic cross section). The implication is that the cross section (per Ni atom) for a Ni L edge will always asymptote to the same value, irrespective of the environment of the Ni atom. This makes it possible to compare the relative changes in the shape of the Ni L edges recorded in different materials. The analysis is complicated by the possibility of core-level shifts in different systems. This is accounted for by making all measurements with respect to the core-level binding energy, defined by the inflection point at the onset of the Ni L_3 edge. The systematic error made in this definition is at most 0.1 eV, which leads to an error in the measured cross-section of

5 b in the worst case.[97,37] In the following analysis the edge onset is chosen as the zero of the energy axis.

If the edges are scaled so that they all match at energies well above the edge onset (a window between 30 and 40 eV above the edge onset is chosen for the Ni L edges) then all the spectra have the same intensity scale and thickness and detector effects are factored out. Thus comparisons of the relative cross sections per Ni atom can be made. The measurements can be placed on an absolute scale by noting that all the Ni spectra must match the atomic Ni cross section well beyond the edge onset. (The LAPW band structures discussed in Sec. VI B do not cover a wide enough energy range for a general comparison to be made.)

After background subtraction and deconvolution of multiple scattering, the spectra are scaled to the HS cross section for a Ni atom[77] (supplied by P. Rez). The cross-section is calculated for a 100-keV electron beam, a probe convergence angle of 10 mrad, and a collection angle of 16 mrad which are the same conditions used to acquire the measured spectra. If the intensity of the measured spectrum after background subtractions is $I(E)$ and the free-atom differential cross section is $d\sigma(E)/dE$, then the measured spectrum is scaled by a factor

$$M=\frac{\int_{30\ \mathrm{eV}}^{40\ \mathrm{eV}}(d\sigma(E)/dE)\,dE}{\int_{30\ \mathrm{eV}}^{40\ \mathrm{eV}}I(E)dE} \tag{B1}$$

to convert it to a cross section (the L_3-edge onset at approximately 852-eV energy loss is chosen as the zero of the energy axis in this analysis). The integration window between 30 and 40 eV above L_3-edge onset is chosen as it also lies sufficiently beyond the L_2 edge so that the oscillations in the EELS fine structure have been damped. The remaining extended fine structure is slowly varying and oscillatory about the atomic cross section.[4] This makes it possible to convert a measured spectrum to a cross section per Ni atom. Consequently, thickness differences are corrected and any changes in shape are measured relative to an isolated Ni atom. Of course, for this to work, multiple-scattering effects must first be removed and this is done using the Fourier ratio deconvolution mentioned earlier. An important point to note is that the calculated HS cross section includes only transitions to the free-atom continuum and not to the empty atomic d levels. The d levels broaden into bands in the solid which are also not accounted for in the cross sections, which is why the normalization must be performed at high enough energies to be independent of the d bands.

The integrated cross sections obtained by applying the normalizing factor of Eq. (B1) to the measured spectra,

$$I_x=\int_{-5\ \mathrm{eV}}^{35\ \mathrm{eV}}\frac{d\sigma_x(E)}{dE}dE\approx M\int_{-5\ \mathrm{eV}}^{35\ \mathrm{eV}}I_x(E)dE, \tag{B2}$$

are given in Table I. The range of integration from -5 to 35 eV beyond the L_3-edge onset includes the near-edge regions of both the L_2 and L_3 Ni edges. The *absolute* values should not be taken too seriously as the atomic model is not appropriate close to the edge onset. However *relative* differences between measurements for the same type of atom are significant as the same systematic error has been made in each measurement.

TABLE V. Broadening parameters for the Ni and Al L edges. All values are in eV.

	Ni L_3 Γ_c	Ni L_2 Γ_c	Al $L_{2,3}$ Γ_c	E_p	E_F-E_0
Ni	0.5	1.4	-	4	9
Ni_3Al	0.5	1.4	0.004	5	9
NiAl	0.5	1.4	0.004	20	9
Al	-	-	0.004	-	-

APPENDIX C: CORE HOLE AND QUASIPARTICLE LIFETIMES

In order to compare the calculated Kohn-Sham eigenvalues to the experimentally measured EELS spectra, we must account for the finite lifetimes of the excitations. These lifetimes broaden the initial and final states. The treatment of the lifetime effects closely follows that of Müller and Wilkins.[4] The broadening of the spectrum due to the core-hole width Γ_c is

$$\overline{M}(E)=\frac{\Gamma_c}{2\pi}\int_{-\infty}^{+\infty}\frac{M(E')dE'}{(E-E')^2+(1/4)\,\Gamma_c^2}, \tag{C1}$$

and the final-state lifetime adds an additional, energy-dependent broadening, $\Gamma_Q(E)$:

$$\overline{\overline{M}}(E)=\frac{1}{2\pi}\int_{-\infty}^{+\infty}\frac{\Gamma_Q(E')\overline{M}(E')dE'}{(E-E')^2+(1/4)\,\Gamma_Q(E')^2}. \tag{C2}$$

The core-hole lifetimes for the Ni and Al L edges have been tabulated.[112] The quasiparticle lifetime is less well characterized, so it is estimated using the random phase approximation[113]

$$\Gamma_Q(E)=\frac{\pi^2\sqrt{3}}{128}E_p\left(\frac{E-E_F}{E_F-E_0}\right)^2, \tag{C3}$$

where E_F is the Fermi energy, E_0 is the bottom of the valence band, and E_p is the plasmon energy. The plasmon energy is taken from experimental measurements of the dielectric function determined from the EELS valence spectra. The Al densities of states have large peaks 10–20 eV above the Fermi energy, and a low DOS in the region of interest near the Fermi energy. Equation (C3) is valid only for small $E-E_F$ and leads to large errors when applied to the Al DOS. Consequently only the core-hole and instrumental broadenings are applied to the Al DOS to simulate the experimental spectra, while all three effects are used to simulate the Ni L edges.

Finally the spectra are convolved with a Gaussian whose width σ_I corresponds to the instrumental resolution after Wiener filtering. For the Ni Ledges, the instrumental resolution was 0.8-eV full width at half maximum, and, for the Al L edges, the resolution was 0.5 eV. The broadening parameters are given in Table V. The broadened DOS and oscillator strengths are shown in Figs. 12 and 13.

[1] D. A. Muller, S. Subramanian, S. L. Sass, J. Silcox, and P. E. Batson, Phys. Rev. Lett. **75**, 4744 (1995).
[2] H. W. B. Skinner, Philos. Trans. R. Soc. London, Ser. A **239**, 95 (1940).
[3] D. J. Nagel, D. A. Papaconstantopoulos, J. McCaffery, and J. Criss, in *Proceedings of the International Symposium on X-Ray Spectra and Electronic Structure of Matter*, edited by A. Faesler and G. Weich (Academic, New York, 1973), p. 51.
[4] J. E. Müller and J. Wilkins, Phys. Rev. B **29**, 4331 (1984).
[5] R. D. Leapman, L. A. Grunes, and P. J. Fejes, Phys. Rev. B **26**, 614 (1982).
[6] P. Lerch, T. Jarlborg, V. Codazzi, G. Loupias, and A. M. Flank, Phys. Rev. B **45**, 11 481 (1992).
[7] P. E. Batson, Nature (London) **366**, 728 (1993).
[8] N. D. Browning, M. M. Chisholm, and S. J. Pennycook, Nature (London) **366**, 143 (1993).
[9] D. A. Muller, Y. Tzou, R. Raj, and J. Silcox, Nature (London) **366**, 725 (1993).
[10] D. M. Pease and L. V. Azaroff, J. Appl. Phys. **50**, 6605 (1979).
[11] J. C. Fuggle and J. E. Inglesfield, *Unoccupied Electronic States*, Topics in Applied Physics Vol. 69 (Springer-Verlag, Berlin, 1992).
[12] V. L. Moruzzi, A. R. Williams, and J. F. Janak, Phys. Rev. B **10**, 4856 (1974).
[13] D. Hackenbracht and J. Kubler, J. Phys. F **10**, 427 (1980).
[14] K. Pechter, P. Rastl, A. Neckel, R. Eibler, and K. Schwarz, Monatsch. Chem. **112**, 317 (1981).
[15] D. Sarma, W. Speier, R. Zeller, E. van Leuken, R. A. de Groot, and J. C. Fuggle, J. Phys.: Condens. Matter **1**, 9131 (1989).
[16] S. C. Lui, J. W. Davenport, E. W. Plummer, D. M. Zehner, and G. W. Fernando, Phys. Rev. B **42**, 1582 (1990).
[17] V. L. Moruzzi and P. M. Marcus, Phys. Rev. B **42**, 5539 (1990).
[18] J. H. Xu, B. I. Min, A. J. Freeman, and T. Oguchi, Phys. Rev. B **41**, 5010 (1990).
[19] T. Nautiyal and S. Auluck, Phys. Rev. B **45**, 13 930 (1992).
[20] C. L. Fu and M. H. Yoo, Acta Metall. Mater. **40**, 703 (1992).
[21] C. L. Fu and M. H. Yoo, Mater. Chem. Phys. **32**, 25 (1992).
[22] S. Sun, N. Kioussis, S. P. Lim, A. Gonis, and W. H. Gourdin, Phys. Rev. B **52**, 14 421 (1995).
[23] C. Colinet, A. Bessoud, and A. Pasturel, J. Phys.: Condens. Matter **1**, 5837 (1989).
[24] F. Szmulowicz and D. Pease, Phys. Rev. B **17**, 3341 (1978).
[25] N. V. Smith, C. T. Chen, F. Sette, and L. F. Mattheiss, Phys. Rev. B **46**, 1023 (1992).
[26] T. K. Sham, Solid State Commun. **64**, 1103 (1987).
[27] D. J. Nagel, L. L. Boyer, D. A. Papaconstantopoulos, and B. M. Klein, in *Proceedings of the International Conference on Transition Metals*, IOP Conf. Proc. No. 39 (Institute of Physics, Toronto, 1978), p. 104.
[28] G. A. Botton and C. J. Humphreys, in *Proceedings of ICEM 13-PARIS*, edited by B. Jouffrey and C. Colliex (Les Editions de Physique, Paris, 1994).
[29] G. A. Botton, G. Y. Guo, W. M. Temmerman, and C. J. Humphreys, Phys. Rev. B **54**, 1682 (1996).
[30] D. A. Muller, P. E. Batson, S. Subramanian, S. L. Sass, and J. Silcox, in *Defect-Interface Interactions*, edited by E. P. Kuam, A. M. King, M. J. Mills, T. D. Sands, and V. Vitek, MRS Symposium Proceedings, No. 319 (Material Research Society, Pittsburgh, 1994), p. 299
[31] D. A. Muller, S. Subramanian, S. L. Sass, J. Silcox, and P. E. Batson, in *Proceedings of ICEM 13-PARIS* (Ref. 28).
[32] D. A. Muller and J. Silcox, Philos. Mag. A **71**, 1375 (1995).
[33] C. H. Muller, H. Wonn, W. Blau, P. Ziesche, and V. P. Krivitskii, Phys. Solid State **95**, 215 (1979).
[34] D. J. Singh, Phys. Rev. B **46**, 14 392 (1992).
[35] N. F. Mott, Adv. Phys. **13**, 325 (1964).
[36] A. E. Carlsson, Phys. Rev. B **40**, 912 (1989).
[37] D. A. Muller, P. E. Batson, and J. Silcox (unpublished).
[38] D. Nguyen-Manh, D. Mayou, A. Pasturel, and F. Cyrot-Lackman, J. Phys. F **15**, 1911 (1985).
[39] D. G. Pettifor and M. Aoki, Philos. Trans. R. Soc. London, Ser. A **334**, 439 (1991).
[40] M. Aoki, Phys. Rev. Lett. **71**, 3842 (1993).
[41] A. P. Horsfield, A. M. Bratkovsky, M. Fearn, D. G. Pettifor, and M. Aoki, Phys. Rev. B **53**, 12 694 (1996).
[42] D. A. Muller (unpublished).
[43] J. Friedel, Philos. Mag. **43**, 153 (1952).
[44] V. Heine, in *Solid State Physics*, edited by H. Ehrenreich and F. Seitz (Academic, New York, 1980), Vol. 35, p. 1.
[45] R. Hoffmann, *Solids and Surfaces: A Chemists View of Bonding in Extended Structures* (VCH, New York, 1988).
[46] A. P. Sutton, *Electronic Structure of Materials* (Clarendon, Oxford, 1993).
[47] D. G. Pettifor, *Bonding and Structure of Molecules and Solids* (Clarendon, Oxford, 1995).
[48] P. W. Atkins, *Physical Chemistry*, 2nd ed. (Freeman, San Francisco, 1982).
[49] R. S. Mulliken, J. Chem. Phys. **23**, 1833 (1955).
[50] D. Sanchez-Portal, E. Artacho, and J. M. Soler, Solid State Commun. **95**, 685 (1995).
[51] M. D. Segall, C. J. Pickhard, R. Shah, and M. C. Payne, Mol. Phys. **89**, 571 (1996).
[52] D. J. Singh, *Plane Waves, Pseudopotentials, and the LAPW Method* (Kluwer, Boston, 1994).
[53] P. A. Schultz and J. W. Davenport, Scr. Metall. **27**, 629 (1992).
[54] O. K. Anderson, O. Jepsen, and D. Glotzel, in *Highlights of Condensed Matter Theory Course LXXXIX*, edited by F. Bassani, F. Fermi, and M. P. Tosi (North-Holland, Amsterdam, 1985).
[55] E. P. Wigner and F. Seitz, Phys. Rev. **46**, 509 (1934).
[56] O. K. Anderson, O. Jepsen, and M. Sob, in *Electronic Band Structure and its Applications*, edited by M. Yussouff, Lecture Notes in Physics (Springer, Berlin, 1987), Vol. 283.
[57] D. G. Pettifor, in *Electron Theory in Alloy Design*, edited by D. G. Pettifor and A. Cottrell (Alden, Oxford, 1992).
[58] H. A. Bethe, Ann. Phys. (Leipzig) **5**, 325 (1930).
[59] H. A. Bethe and E. E. Salpeter, *Quantum Mechanics of One and Two Electron Atoms* (Springer, Berlin, 1957).
[60] M. Inokuti, Rev. Mod. Phys. **43**, 297 (1971).
[61] J. J. Sakurai, *Modern Quantum Mechanics* (Addison-Wesley, New York, 1985).
[62] Although this work will only consider cases where the dipole contribution dominates the EELS signal (a function of our detector geometry), there is also a generalized oscillator strength (GOS) for general scattering angles. The GOS reduces to the optical oscillator strength when the momentum transfer is predominantly in the forward direction, i.e., $q \rightarrow (q_{\min} = k_0 \theta_E)$ (Refs. 58 and 60).
[63] M. Isaacson and M. Umlaut, Optik (Stuttgart) **50**, 213 (1978).
[64] R. E. Burge and D. L. Misell, Philos. Mag. **18**, 251 (1968).
[65] D. H. Tomboulian, in *Handbuch der Physik*, edited by S. Flügge (Springer, Berlin, 1957), Vol. 30, p. 46.
[66] L. G. Parratt, Rev. Mod. Phys. **31**, 616 (1959).

[67] While the Ni *M* edge is also accessible by EELS, analysis of the fine structure is complicated by the presence of a Fano resonance.
[68] The EELS cross section per Ni atom for an 860-eV energy loss of a 100-keV electron is roughly 10 b/eV, which corresponds to a mean free path of about 1 cm in Ni, while the mean free path for an 860-eV x-ray in Ni is about 10 nm.
[69] R. F. Egerton, *Electron Energy Loss Spectroscopy in the Electron Microscope*, 2nd ed. (Plenum, New York, 1996).
[70] D. McMullan, P. J. Fallon, Y. Ito, and A. J. McGibbon, *Proceedings of EUREM 92* [Electron Microsc. **1**, 103 (1992)].
[71] R. F. Egerton, B. G. Williams, and T. G. Sparrow, Proc. R. Soc. London, Ser. A **398**, 395 (1985).
[72] W. Press, B. Flannery, S. Teukolsky, and W. Vetterling, *Numerical Recipes*, 1st ed. (Cambridge University Press, Cambridge, 1988).
[73] K. Wong, Ph.D. thesis, Cornell University, NY, 1994.
[74] The differences between the L_2 and L_3 transitions result from a spin-orbit splitting in the valence band. As this splitting (about 80 meV) is much smaller than the bandwidth (about 4 eV) in all the alloys studied here, it has little effect on the cohesive and structural trends of interest.
[75] M. Brown, R. E. Peierls, and E. A. Stern, Phys. Rev. B **15**, 738 (1977).
[76] L. F. Mattheiss and R. E. Dietz, Phys. Rev. B **22**, 1663 (1980).
[77] R. D. Leapman, P. Rez, and D. F. Mayers, J. Chem. Phys. **72**, 1232 (1980).
[78] R. E. Dietz, E. McRae, Y. Yafet, and C. Caldwell, Phys. Rev. Lett. **33**, 1372 (1974).
[79] P. Hohenberg and W. Kohn, Phys. Rev. **136**, 864 (1964).
[80] W. Kohn and L. Sham, Phys. Rev. A **140**, 1133 (1965).
[81] L. Hedin and S. Lundqvist, in *Solid State Physics*, edited by H. Ehrenreich and F. Seitz (Academic, New York, 1969), Vol. 23.
[82] J. E. Müller, O. Jepsen, and J. W. Wilkins, Solid State Commun. **42**, 365 (1982).
[83] L. J. Sham and W. Kohn, Phys. Rev. **145**, 561 (1966).
[84] P. Horsch, W. von der Linden, and W. D. Lukas, Solid State Commun. **62**, 359 (1987).
[85] R. Godby, M. Schlüter, and L. J. Sham, Phys. Rev. B **37**, 10 159 (1988).
[86] F. R. de Boer, C. J. Schinkel, J. Biesterbos, and S. Proost, J. Appl. Phys. **40**, 1049 (1969).
[87] N. Buis *et al.*, Phys. Lett. **56A**, 115 (1976).
[88] H. J. Monkhorst and J. D. Pack, Phys. Rev. B **13**, 5188 (1976).
[89] N. W. Ashcroft, Phys. Rev. B **19**, 4906 (1979).
[90] F. Szmulowicz and B. Segall, Phys. Rev. B **21**, 5628 (1980).
[91] W. Speier, J. C. Fuggle, R. Zeller, B. Ackermann, K. Szot, F. U. Hillebrecht, and M. Campagna, Phys. Rev. B **30**, 6921 (1984).
[92] T. I. Morrison, M. B. Brodsky, N. J. Zaluzec, and L. R. Sill, Phys. Rev. B **32**, 3107 (1985).
[93] D. H. Pearson, B. Fultz, and C. Ahn, Appl. Phys. Lett. **53**, 1405 (1988).
[94] D. H. Pearson, C. Ahn, and B. Fultz, Phys. Rev. B **47**, 8471 (1993).
[95] A. Bzowski and T. K. Sham, Phys. Rev. B **48**, 7836 (1994).
[96] B. T. Thole and G. van der Laan, Phys. Rev. B **38**, 3158 (1988).
[97] D. A. Muller, Ph.D. thesis, Cornell University, 1996.
[98] W. Speier, R. Zeller, and J. C. Fuggle, Phys. Rev. B **32**, 3597 (1985).
[99] D. Mayou, D. Nguyen-Manh, A. Pasturel, and F. Cyrot-Lackmann, Phys. Rev. B **33**, 3384 (1986).
[100] F. Cyrot-Lackmann, Adv. Phys. **16**, 393 (1967).
[101] D. G. Pettifor, Phys. Rev. Lett. **63**, 2480 (1989).
[102] D. G. Pettifor *et al.*, Mater. Sci. Eng. A **192/93**, 24 (1995).
[103] D. G. Pettifor, Commun. Phys. **1**, 141 (1976).
[104] A. R. Mackintosh and O. K. Anderson, in *Electrons at the Fermi Surface*, edited by M. Springford (Cambridge University Press, London, 1980), Chap. 5.3.
[105] F. Ducastelle and F. Cyrot-Lackmann, J. Phys. Chem. Solids **31**, 1295 (1970).
[106] P. W. Anderson, Phys. Rev. **181**, 25 (1969).
[107] W. A. Harrison, *Electronic Structure and the Properties of Solids* (Dover, New York, 1989).
[108] J. A. Moriarty, Phys. Rev. B **38**, 3199 (1988).
[109] S. M. Foiles, Phys. Rev. B **48**, 4287 (1993).
[110] H. Jones, N. F. Mott, and H. W. B. Skinner, Phys. Rev. **45**, 379 (1934).
[111] F. Ducastelle and F. Cyrot-Lackmann, J. Phys. Chem. Solids **32**, 285 (1971).
[112] M. O. Krause and J. H. Oliver, J. Phys. Chem. Ref. Data **8**, 329 (1979).
[113] D. Pines and P. Nozieres, *The Theory of Quantum Liquids* (Addison-Wesley, New York, 1989), Vol. 1.
[114] S. Subramanian, D. A. Muller, J. Silcox, and S. L. Sass, Acta Mater. **45**, 3565 (1997).